

LIMNOLOGY and OCEANOGRAPHY



Limnol. Oceanogr. 65, 2020, 260–288 © 2019 The Authors. Limnology and Oceanography published by Wiley Periodicals, Inc. on behalf of Association for the Sciences of Limnology and Oceanography. doi: 10.1002/lno.11296

Mixing processes in small arctic lakes during spring

Alicia Cortés , 1* Sally MacIntyre 10,12

¹Marine Science Institute, University of California, Santa Barbara, California

²Department of Ecology, Evolution, and Marine Biology, University of California, Santa Barbara, California

Abstract

Small ice-covered lakes are stratified by temperature and solutes. Using time series measurements and profiles of temperature, specific conductance (SC), and dissolved oxygen obtained during spring 2014 and 2015, we identified the physical processes occurring under the ice and at ice-off in two ~ 2 ha, 10-m-deep arctic lakes. The lakes are distinguished from other freshwater, ice-covered lakes by solutes initially stabilizing the density stratification when temperature decreased in the lower water column and, with one exception, stabilizing it during warming. With an ice cover 1 m thick, wind-forced internal waves occurred, with 2nd vertical mode waves prevalent where stratification was weak. Snowmelt induced near-surface chemical stratification such that diurnal thermoclines formed with stable temperature stratification in a ~ 4-m-thick layer. Horizontal exchange was mediated by internal waves and gravity currents induced by greater heating near shore and as incoming snowmelt displaced water in shallow regions. Toward ice-off, the gravity currents reduced temperature stratification between the snowmelt-induced near-surface pycnocline and the bottom pycnocline but slight increases in SC precluded radiatively driven convection. Snowmelt retention was greater with rapid spring heating. The lakes did not mix by ice-off. With moderate winds, Wedderburn numbers decreased below 3 at ice-off, and the nearsurface pycnocline upwelled and then deepened due to internal wave-induced mixing. The concomitant downward mixing of heat caused a rapid onset of thermal stratification, and that, combined with incomplete mixing under the ice, led to persistence of near-bottom depletion in oxygen and increased density and dissolved solutes.

Arctic lakes have long periods of ice-cover that can lead to thick ice and large, near-surface temperature gradients relative to boreal and temperate locations (Barnes and Hobbie 1960; Farmer 1975; Duguay et al. 2003), oxygen depletion in the lower water column (Bengtsson et al. 1996; Terzhevik et al. 2009; Kirillin et al. 2012), and accumulation of $\rm CO_2$ and $\rm CH_4$ (MacIntyre et al. 2018a). The extent of mixing under the ice and at ice-off will determine whether anoxia persists and greenhouse gases evade. Despite the seminal work of Mortimer and Mackereth (1958), few studies of the processes causing transport and mixing have been conducted in arctic lakes during winter and even fewer in spring (Barnes and Hobbie 1960; Welch and Bergmann 1985; Kirillin et al. 2015). The considerable literature for temperate lakes between 43°N and 66.5°N indicates that radiatively driven convection (RDC) typically

This is an open access article under the terms of the Creative Commons Attribution-NonCommercial-NoDerivs License, which permits use and distribution in any medium, provided the original work is properly cited, the use is non-commercial and no modifications or adaptations are made.

Additional Supporting Information may be found in the online version of this article.

causes mixing under the ice in spring (Farmer 1975; Mironov et al. 2002). This one-dimensional (1D) process is expected to dominate unless the lakes have extensive shallow regions (Farmer 1975). Both the 1D penetrative convection, induced when increased solar radiation at temperatures below 4°C creates instabilities, and horizontal convection, induced by greater heating nearshore, can transport oxygen deep in the water column and alleviate anoxia (Stefanovic and Stefan 2002; Rizk et al. 2014; Yang et al. 2017). Because solutes contribute to the density of freshwaters near 4°C (Malm et al. 1998; MacIntyre et al. 2018a), chemical stratification may stabilize the water column despite the increases in temperature induced by solar radiation. If such occurs, other processes besides penetrative convection may moderate the transport of heat and solutes under the ice. Their efficacy will determine the fate of solutes produced under the ice.

Small arctic lakes in which respiration over the winter causes gradients in solutes under the ice provide an opportunity to determine how chemical stratification moderates transport below the ice and mixing at ice-off (Cortés et al. 2017; MacIntyre et al. 2018a). Solutes produced by sediment respiration over the winter are concentrated near the bottom by downslope gravity currents (Mortimer and Mackereth 1958; Malm et al. 1997).

^{*}Correspondence: alicia.cortes@ucsb.edu

Mid-water column, intrusions of solutes occur in small, metabolically active lakes when the rate of density increase near the bottom is rapid in early winter (MacIntyre et al. 2018a). Cryoconcentration, and the resultant downward mixing of solutes, may cause gradients under the ice (Malm et al. 1997; Granin et al. 1999; Bluteau et al. 2017). These gradients may be reversed and intensified by incoming snowmelt which creates near-surface pycnoclines (Pieters and Lawrence 2009: Cortés et al. 2017). The influence of increased solutes on density will be larger when temperatures are closer to 4°C, hence between-year differences in temperature under the ice in small lakes may lead to between-year variations in physical processes (Malm 1998; Salonen et al. 2014; MacIntyre et al. 2018a). How increases in solutes below the ice and mid-water column modify density structure and the physical processes operative in spring has not been quantified.

The changes in distribution of solutes and heat during spring may further modify physical processes. Inputs of fresher water in spring are expected to inhibit or delay the onset of penetrative convection (Pieters and Lawrence 2009; Cortés et al. 2017), and increased near-bottom density gradients may reduce the efficacy of RDC, which has been shown to energize a near-bottom internal wave field (Mironov et al. 2002; Bouffard et al. 2016). The changing distribution of heat and solutes may also moderate the density structure in ways that enable internal waves. Evidence does exist for barotropic and baroclinic seiches and the currents and horizontal dispersion they induce during winter (Bengtsson 1996; Malm et al. 1998; Petrov et al. 2006) as well as for rotational waves that are expected in all but the smallest lakes (Kirillin et al. 2009, 2012). However, internal waves are not expected in spring due to thicker ice cover and when penetrative convection erodes stratification (Kirillin et al. 2012). That said, they may be forced by wind if stratification is weak and persists and by gravity currents caused by nearshore heating. A more comprehensive understanding of the physical processes in spring that moderate warming and the pathways of snowmelt requires studies in ice-covered lakes in which temperature and depth dependent variations in solute concentrations cause variations in density stratification.

If penetrative convection or other processes occurring under ice in spring do not mix the water column, mixing at ice-off would be required to alleviate anoxia and redistribute solutes in the lower water column. Wind-induced nonlinear waves with their increased shear may be critical. The degree of nonlinearity can be predicted from the Wedderburn number, W, and the related Lake number, L_N (Imberger and Patterson 1990). These indices are ratios of buoyancy forces that reduce mixing to inertial ones that cause it; mixing is more effective with shallower or deeper thermoclines relative to mean depth or with longer fetch. As guidelines, W > 10 implies minimal thermocline tilting, 1 < W < 10 partial tilting, and W < 1 full upwelling. Internal waves become progressively more nonlinear, such that more mixing occurs, as W and L_N decrease (Horn et al. 2001;

Boegman et al. 2005a). Thus, depending on the wind speeds at ice-off, nonlinear waves may contribute to the transfer of heat and solutes in the water column. The extent to which near-surface chemoclines induced by snowmelt or ice melt make internal wave-induced mixing more difficult will likely depend on specific conductance within the lake and the extent of heating of the fresher, near-surface water (Pieters and Lawrence 2009). The duration of mixing will be an important control on the extent to which density gradients near the sediments are eroded, anoxia is alleviated, greenhouse gases are dispersed, and CH₄ oxidized.

The hydrodynamics of ice-covered lakes is a neglected area of modern limnology (Kirillin et al. 2012). Improved capabilities with sensors and new instruments have now enabled studies throughout the ice-covered period (Kirillin et al. 2015; Cortés et al. 2017; Yang et al. 2017), yet many questions remain. We used data from high-resolution instrumentation to analyze physical processes operative under the ice from early spring until ice-off in two small arctic lakes in 2014 and 2015. Metabolically active during the ice-covered period, the two lakes differed in stratification at the onset of warming in spring and in morphometry, with one having a deep and a shallow subbasin. We characterize the processes with time series measurements and profiles of temperature, specific conductance, and dissolved oxygen with instrument arrays and profiles along transects. We further interpret changes with concomitant measurements of meteorology, ice thickness, and snow depth. Our focus is on the depths and magnitude of RDC, changes in stratification and internal waves under the ice, influence of snowmelt, and horizontal exchange. We further focus on internal wave driven mixing prior to and after ice-off.

Study sites

The two lakes are oligotrophic kettle lakes located on the northern foothills of the Brooks Range, Alaska (Fig. 1) (Hobbie et al. 1995; Luecke et al. 2014). Lake N2 (68°38'N, 149°37'W; surface area S_A = 1.6 ha, maximum depth, z_{max} = 10.3 m, mean depth $z_{\text{mean}} = 5 \text{ m}$, total volume $V = 81 \times 10^3 \text{ m}^3$, and catchment area CA = 21.7 ha) and is ~ 600 m northwest of Toolik Lake. (Fig. 1a,b). Lake E1 (68°37′N, 149°33′W; $S_A = 2.8$ ha, $z_{max} = 11.5$ m, $z_{\text{mean}} = 3 \text{ m}$, $V = 90 \times 10^3 \text{ m}^3$, CA = 88.4 ha) is 1.5 km east of Toolik Lake (Fig. 1c,d). The deepest part of Lake (L.) N2 is to the west, with bottom slopes of ~ 6% to the east and 20% to the west. A small braided stream enters from the east and exits to the north. L. E1 has two subbasins separated by a shallow 3 m ridge. The deepest basin is on the eastern side of the lake. A small braided stream enters near the east and exits from the west. Discharge from both streams was measured after peak flow and within a week of ice-off. Incoming values were $\sim 10 \, \mathrm{L \ s^{-1}}$ in L. N2 and ~ 50 L s⁻¹ in L. E1 and outgoing flows were up to twice as high (Caitlin Rushlow, pers. comm.). The topography around L. N2 partially shelters it from southerly winds and enables

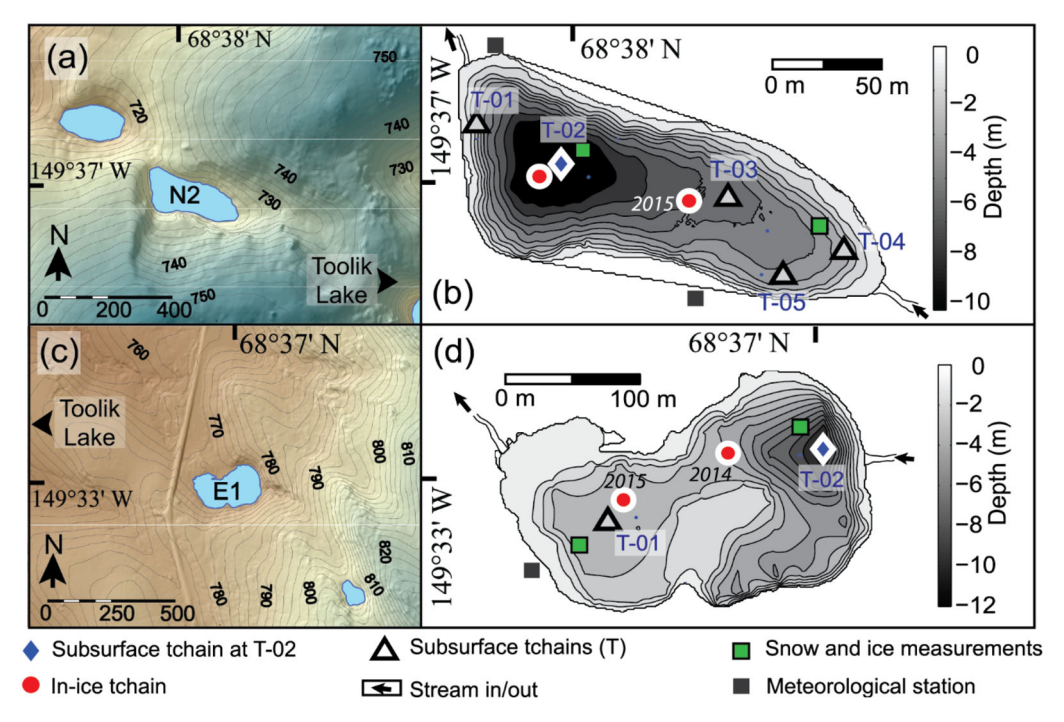


Fig. 1. (a, c) Topographic maps for watersheds of Lakes N2 and E1; contours at 2 m intervals. (b, d) Bathymetric maps of Lakes N2 and E1; contours at 1 m intervals. Arrows mark location of incoming and outgoing streams. Deepest subsurface array (T-02, blue diamonds), in-ice arrays (red dots), and additional subsurface arrays (black triangles). Locations where snow and ice thickness were measured are shown with green squares. Meteorological stations (black squares).

greater flow over the western half of the lake by northerly and northwesterly winds. These differences in exposure were expected to modify snow depth and the persistence of snow cover on the lake. L. E1 has greater exposure to winds from the west and the hills surrounding it are less steep than those around L. N2. The lakes are typically ice-covered from around mid-September to mid-June.

Methods and calculations

Meteorology, ice thickness, and bathymetry

Meteorological data were obtained from stations on the northwestern and southeastern shores of L. N2 (Fig. 1b). Instrumentation included sensors measuring wind speed and direction (accuracy 1.1 m s⁻¹ and resolution 0.5 m s⁻¹) at 2 m height, a shielded air temperature sensor (0.2°C accuracy) and relative humidity sensor (accuracy 2.5% of the reading). Data were sampled every second and averaged for 5 min. Similar meteorological instrumentation was deployed on the western shore of L. E1 (Fig. 1d). A station 50 m to the east of Toolik Lake provided incoming and outgoing short- and long-wave radiation as well as additional 5 min averaged air temperature, relative humidity, wind speed, and direction (Cortés et al. 2017). Between-station differences in wind direction were at most 5°. Gaps in the meteorological data were filled using data from the Toolik Lake station after linear regressions established relations between the sites during periods with overlapping data. Snow

depth and ice thickness on the lakes were measured monthly in winter and every one or two weeks in spring. Bathymetric data were collected with a Garmin GPSMAP 188 sounder and Sonar Mit echo sounder (J. Stuckey and R. Fulweber, unpubl. data).

Moored instrumentation

Time series measurements of temperature, specific conductance (SC), and dissolved oxygen (O2) were obtained from sensors on taut-line moorings below the ice deployed prior to iceon each fall (Fig. 1b,d). We deployed subsurface arrays in L. E1 at a deep and a shallow site and up to four under-ice arrays along the main axis of L. N2 with an additional one to the southeast. Arrays were numbered from west to east, and the array at the deepest location was T-02 in both lakes. The temperature sensors in L. N2 on all arrays were RBR TR-1050 with 0.002°C accuracy and resolution an order of magnitude higher. In L. E1, RBR TR-1050 sensors were used in the deep basin, and Onset HOBO Water Temp Pros were used in the shallow one with the latter having 0.2°C accuracy and 0.02°C resolution. Specific conductance was measured with Onset U24-001 sensors. For further details about instrumentation and calibration, see Cortés et al. (2017). Dissolved oxygen was measured with optical sensors (PME MiniDOT loggers, accuracy of 5% of measurement or 0.3 mg L⁻¹, whichever is larger, and resolution of 0.01 mg L⁻¹). In-ice arrays were deployed through the ice in November of each year. Arrays had Onset HOBO Water Temp Pro temperature sensors at 0.25 m intervals and Onset U24-001 specific conductance sensors positioned 1.75 m below the ice on deployment. For L. N2, arrays were deployed near T-02 in both years and additionally near T-03 in 2015. The in-ice arrays were deployed in the deep basin in 2014 and in the shallow basin in 2015 in L. E1. Instrument depths are indicated in the figures to follow. The in-ice temperature records also enabled estimation of changes in ice thickness ($h_{\rm ice}$) with 0.25 m resolution.

Profiling data

Profiles of conductivity, temperature, depth (CTD), and dissolved oxygen were obtained weekly at the deepest sites beginning prior to snowmelt and continuing at least a week after ice-off (Fig. 1). We used a Hydrolab DS5 water column profiler and sampled at 1 m intervals, YSI Castaway with vertical resolution of ~ 0.3 m, and a JFE Advantech profiler with RINKO optical dissolved oxygen electrode. Vertical resolution was 0.1 m and ~ 0.025 m in 2014 and 2015, respectively. The Hydrolab DS5 profiler also measured pH and irradiance with a LiCor 2 pi collector. Profile data also were used to check the calibration of the sensors on arrays, to fill gaps in our time series measurements, and for improved contouring of the time series SC and O_2 data. Further details about instrument specifications and data processing are available in Cortés et al. (2017).

Density, Wedderburn, and lake numbers

Density was computed from temperature and salinity following Chen and Millero (1977) with salinity computed from specific conductance (Pawlowicz 2008; Cortés et al. 2017). Salinity calculated by summing major ions was 0.9 times specific conductance of lake water and 0.2 times the specific conductance of snowmelt. Computed densities from Chen and Millero (1977) are identical to those computed using newer algorithms (MacIntyre et al. 2018*b*). Buoyancy frequency (*N*) in cycles per hour (cph) was computed as $N = [(g/\rho \ \Delta \rho/\Delta z)^{1/2} 3600/2\pi]$, where *g* is the acceleration of gravity, $\Delta \rho/\Delta z$ is the vertical density gradient, and ρ is the density of water.

We computed Wedderburn numbers at ice-off as $W = [(g \Delta \rho)]$ h^2) / $(\rho u_{*w}^2 L)$], where $\Delta \rho$ is the density difference across the thermocline, h is the thickness of the surface mixed layer, u_{*w} is the water friction velocity computed from shear stress from wind, and L is the length of the lake in the direction of the wind (Imberger and Patterson 1990). For this calculation, $\Delta \rho$ was computed from temperature and SC in the mixed layer above the thermocline and at a depth just above the near-bottom chemocline. Lake numbers (L_N) at ice-off were computed following Imberger and Patterson (1990) using density profiles for the full water column. Lake numbers were averaged over an hour, a fourth of the dominant internal wave period calculated following Gill (1982). We assume equivalency of W and L_N (Stevens and Lawrence 1997; MacIntyre et al. 1999). The speed at which snowmelt flowed across L. N2 was obtained by dividing the distance between under-ice SC loggers in 2015, ~ 100 m, by the difference in time at which abrupt changes in SC occurred.

Heat fluxes and mixing

Penetrative convection is usually identified from time series temperature measurements when the water column becomes isothermal at progressively increasing depths beginning immediately below the surface boundary layer (Farmer 1975) and interior convection when isothermal regions develop deeper in the water column (Malm et al. 1997). Using high-resolution sensors, Yang et al. (2017) inferred active mixing if there were instabilities in the time series data and assumed that isothermy only implied previously mixed water. We similarly expected mixing to occur when the temperature at one depth exceeded that below such that density instabilities formed due to increased temperature below 4°C. If isothermy resulted between the two thermistors over the next several hours, we could assume mixing that had a length scale equal to the separation between thermistors. However, we sometimes found that isothermy did not result even several hours after instabilities formed, and that temperatures increased during periods with isothermy. Thus, we additionally used our array data on transects to determine whether periodic instances of near-isothermy or isothermy itself could be due to other mechanisms than RDC.

We estimated the flux of photosynthetically available radiation (PAR) at a depth z in the water column following Beers Law: I_z = (1- \tilde{a}) 0.45 I_0 $e^{-(kd\ z)}$. In this calculation, \tilde{a} is albedo, we assume PAR is 45% of net shortwave at the surface, I_0 (W m⁻²), there was no snow cover and therefore no reflection from snow, and that the diffuse attenuation coefficient of ice, $k_{\rm d}$ ice, equaled that in the water, k_d . We made this assumption based on the near equivalence of the two terms for black ice obtained when considerable care was taken with the measurements (Belzile et al. 2001). Average and standard deviations of k_d in Lakes E1 and N2 were 0.65 \pm 0.02 m⁻¹ and $0.5 \pm 0.03 \text{ m}^{-1}$, respectively, and were based on 2 to 3 profiles of irradiance under the ice and at ice-off in each year. Given the similarity of values computed for each year, we present the average here. We performed our calculations with range of ã of 0.7 to 0.5, with 0.5 typical at the ice surface when snowfree and dry (Kirillin et al. 2012). We used the albedo which provided the closest match for computed heat flux from solar radiation and from temperature computed over a range of depths using I_z calculated on days during or immediately following dry, windy conditions when we assumed the ice was snowfree.

Heat flux from solar radiation (Q_S , W m⁻²) absorbed within a layer Δz centered at depth z_c , with depth positive downward, over specific time intervals, $\Delta t = t_2 - t_1$, was computed as,

$$Q_{S}(\Delta t, z_{c}) = \frac{1}{\Delta z} \int_{-z_{2}}^{-z_{1}} \left[\sum_{t_{1}}^{t_{2}} I_{z}(t, z) \right] dz$$
 (1)

where the upper boundary $z_1 = (z_c - \Delta z/2)$ and the lower boundary $z_2 = (z_c + \Delta z/2)$. The predicted change in temperature for the time interval was computed as $\Delta T = (Q_S \Delta t)/(\rho \ c_p \ \Delta z)$ where c_p is the specific heat of the water (4,184 J kg⁻¹ °C⁻¹). The predictions were contrasted with the change in temperature for the same time period at z_c . Calculations were done from 06:00 to 20:00 h

to capture diurnal heating and for the 24 h from midnight to midnight.

Heat fluxes from temperature changes in the water column $(Q_T, \text{ in W m}^{-2})$ at specific depths (z_c) were computed from the time-series of temperature (T [t, z]) as,

$$Q_{\mathrm{T}}(\Delta t, z_{\mathrm{c}}) = \rho \cdot c_{\mathrm{p}} \cdot \left[\frac{T(z_{\mathrm{c}}, t_{2}) - T(z_{\mathrm{c}}, t_{1})}{\Delta t} \right] \cdot \Delta z \tag{2}$$

We computed fluxes for 0.3 m layers. Calculations were done on days when changes in temperature in the water column were higher for one to three days than on preceding or following days, as expected when winds had blown snow from the lakes' surface.

Results

The two small arctic lakes were chemically and thermally stratified by spring (Fig. 2). Specific conductance decreased below the ice with this decrease indicative of cryoconcentration (Fig. 2b). A minimum in SC occurred in mid-water column, and then specific conductance increased again, first slowly and then rapidly such that a chemocline was present. Castaway profiles

taken prior to those in Fig. 2 indicated specific conductance below the ice increased and the depth of the SC minimum deepened from late March to late April in both lakes. The ice thickened over this period. Profiles nearshore had slightly elevated SC relative to those offshore. The increased SC below the ice was no longer evident in L. E1 by mid-May and SC increased from the surface downward (Fig. 2e). Both lakes had large gradients in temperature below the ice typical of the surface boundary layer (Fig. 2a,d and Table 1). Temperatures slowly increased below the surface to the bottom in L. N2 in late winter. A mid-water column temperature maximum was present in early spring in L. E1 in both years. In L. N2 in 2014, a temperature maximum developed in the lower water column by ~day of year [dov] 120. The small increases in SC below the temperature maxima stabilized the density structure. Despite the depth dependent changes in temperature and SC, the lakes were stably stratified with stratification least mid-water column (Fig. 2c,f).

Immediately below the ice where SC and temperature both decreased with depth, conditions may have been conducive to weak salt fingering; conditions in the lower water column may have been conducive to double diffusive convection when a temperature maximum was present (Thorpe 2005, 2007). The processes in the water column in spring were more energetic

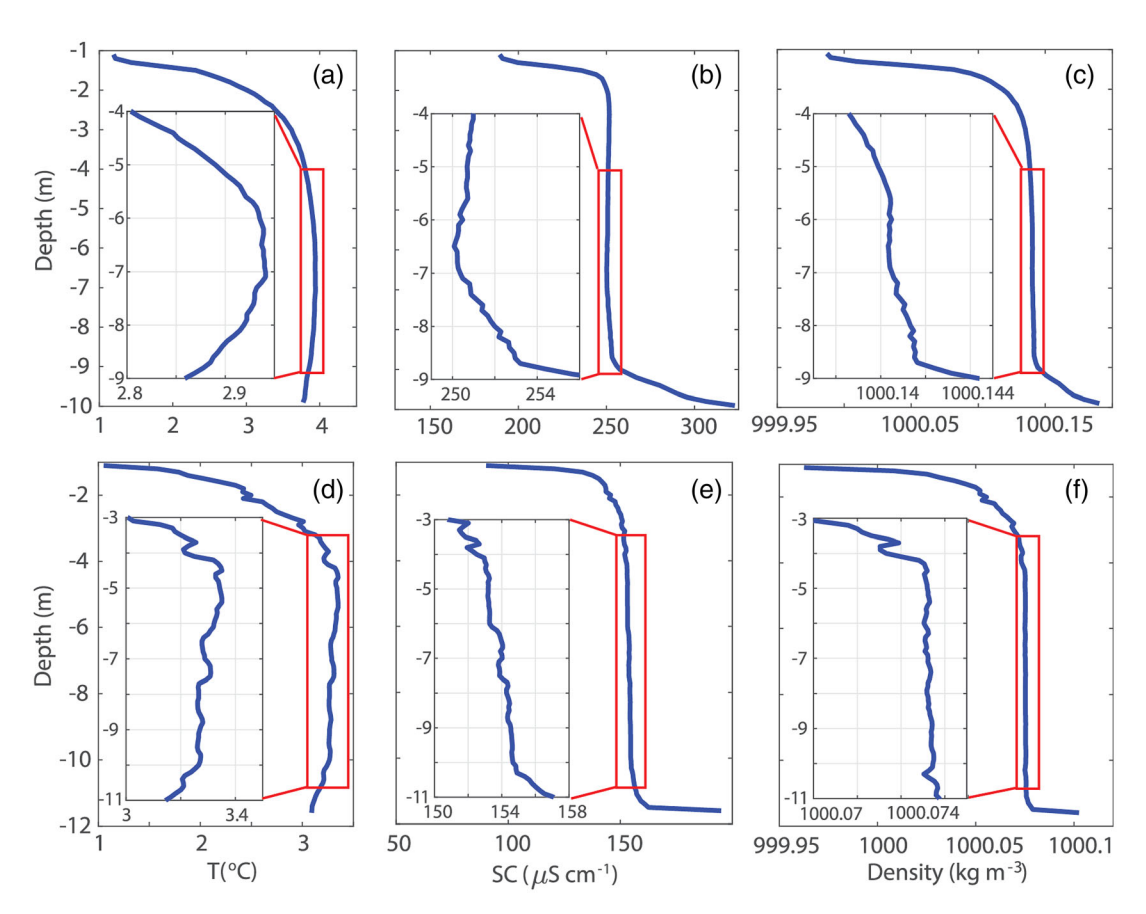


Fig. 2. Profiles of (**a**, **d**) temperature (*T*), (**b**, **e**) specific conductance (SC), and (**c**, **f**) density in L. N2 (a–c) and L. E1 (**d–f**) in early spring 2014 (days 133 and 134, respectively). Data were obtained with a JFE Advantech profiler sampling every 10 cm while free falling.

Table 1. Attributes of lakes in which radiatively driven convection has been noted and our study sites. Latitude, maximum depth z_{max}, surface area S_A, duration of ice cover, and ice thickness. Attributes near the surface during spring under the ice and mid-water column: Thickness of the surface layer; temperature gradient as appropriate for stained lakes in the boreal zone, (Kalff 2002), and extent of the convectively mixing layer CML, h. Temperature and specific conductance SC near the bottom, relevant features during warming under the ice (rate of warming of the convective mixing layer CML, dT_{CML}/dt, and rate of deepening of the dT/dz; buoyancy frequency N; mean temperature T, specific conductance SC, attenuation coefficient K_d directly reported or computed as $K_d = 4.6/8$ ecchi depth, CML, dh_{CML}/dt), and accuracy of the temperature loggers.

							Near surface	urface		Mid-v	Mid-water column	uu		
							dT/d	dT/dz (°C m ⁻¹)						
			j	Duration ice	le cover	Thickness of	Ze o	Relow	2	۱	۶	2	Y	Extent CMI (b)
Lake name	Latitude	(m)	, (km²)	(months)	(m)	surrace layer (m)	ice	ice	(cph)	. (j	$(us cm^{-1})$ (cph)	(cph)	(m)	(m) (m)
Lake Peters*	N°0.69						2	0.05						35
L. N2 2014 [†]	08.6°N	10.3	0.016	6	[1–0.9]	4	7	0.86	[5–25]	3.5	253	[1–3]	0.5	[0]
L. E1 2014 [†]	08.6°N	11.5	0.028	6	[1–0.9]	4	1.5	0.5	[5–25]	3.5	153	[1–3]	0.65	[<u>©</u>
L. E5 2014 [†]	08.6°N	13.0	0.11	6	[1–0.9]	3	4.	0.5	[5-15]	2.8	15	[1–5]	1:1	10
Toolik Lake‡	08.6°N	24.0	1.5	6	[1.2-0.9]	3	8.0	09.0	[5-25]	5.6	100	[1–3]	[0.6-0.7]	[2–11]
Tailings Lake [§]	64.0°N	12.0	0.5	7				0.13		1.5	1450			
Lake Vendyurskoe ^{ll}	62.2°N	13.4	10.4	9	[0.4-0.65]	_	0.5	0.4	ca. 10	<u>-</u> 1	20	5	$[1.1-1.5]^{\ddagger\ddagger\ddagger}$	[4–6]
Lake Rindozero [¶]	62.2°N	9.5	1.8	9	0.67	1.5	0.75	0.42	ca. 15	[1.5–4]	18	4.5	$[2.3-3]^{\$\$\$}$	
Lake Uros [¶]	62.2°N	9.5	4.3	9	0.67			1.1		[04.5]	1	7	0.5	
Lake Onega	61.4°N	30.0	50 (bay)	9~	[0.39-0.41]	_		0.01	4	[0.6-0.9]		[1-2]	[1-1.4] ^{¶¶¶}	[20–28]
(Petrozavodsk Bay)#														
Sombre Lake**	61.0°S	11.2	0.027	6	_			0.15					0.2	[3–7]
Heywood Lake**	61.0°S	6.4	0.045	6	_			0.25		[1.5–3]			0.5	[5–6]
Paajarvi Lake††	61.0°N	75.0	13.4	5	[0.3-0.8]		0.13	[0.02-0.04]		[1–3]		[3–5]	1.5	[20–40]
Lake Velen‡‡	0.009	16.0	2.8		0.5			0.13		[1–2]				9
Babine Lake ^{§§}	55.0°N	200	[300–480]	3	0.4			0.1		[0-3]			0.56	[15–28]
Lake Baikal	51.0°N	1642	31,722	[4–5]				0.03		[2–3]				[20–40]
(south basin,														
100 m deep)""		0	ı		,		,	,		5	,			
Pavilion Lake 🕮	50.0°N	20.0	5		0.46		_	0.01		[2–3]	180			[18–22]
Ryan Lake""	45.0°N	10.0	0.04		[0.3-0.4]			1:1		2				
Lake Simcoe***	44.0°N	42.0	722	[4–5]	[0.2-0.5]	~			7		~200	2	[0.2-0.5]	~[1–3]
Lake Sunapee†††	43.0°N	33.7	16.55	[4–5]		3		0.12		1.5		3	9.0	4

			Penetrative	rative					
	ğ	Bottom	convection	ction		Features	S		
	Temp	SC	dT _{CML} /dt	dh _{cML} /dt	Did horizontal convection deepen weakly	Stepwise increase in the size	Was penetrative convection constrained	Did convection begin deep in the water	Accuracy of temperature loggers
Lake name	(°C)	$(\mu s cm^{-1})$	$(^{\circ}C d^{-1})$	$(m d^{-1})$	stratified zones?	of the eddies?	by snowmelt?	column?	(_° C)
Lake Peters*			0.03	1	9N	Yes	_o N	oN O	
L. N2 2014†	3	200	0	0	Yes	<u>8</u>	Yes	°Z	0.002 (RBR)
L. E1 2014 [†]	3	200	0	0	Yes	<u>8</u>	Yes	°Z	0.002 (RBR)
L. E5 2014 [†]	3.2	100	0.08	0.3	Yes	Yes	8 2	°Z	0.002 (RBR)
Toolik Lake [‡]	3.2	160	0.1	[0.2-1.5]	?	Only below fresh	Yes	°Z	0.002 (RBR)
						lens of water			
Tailings Lake [§]	3.2	160	0.1	[0.2-1.5]	Š	Only below fresh	Yes	°Z	0.002 (RBR)
						lens of water			
Lake Vendyurskoe ^{ll}	5.5	95	[0.1-0.25]	0.2	Š	Yes	_S	Š	0.15
Lake Rindozero [¶]	4.5	80			8	Yes	8	Š	0.05
Lake Uros [¶]	5	25			<u>8</u>	<u>8</u>	8	Yes	0.05
Lake Onega	2.5		0.04	0.3	8 N	Yes	8 N	°N	0.002 (RBR)
(Petrozavodsk Bay)#									
Sombre Lake**	2.5		0.04	0.3	<u>8</u>	Yes	8	°N	0.002 (RBR)
Heywood Lake**					8	Yes	8	Š	
Paajarvi Lake††					Yes	Yes	8 N	°N	
Lake Velen‡‡	3.5		90.0	0.2	<u>8</u>	Yes	8	°N	
Babine Lake ^{§§}				_	<u>8</u>	Yes	8	°N	
Lake Baikal (south basin,					8	Yes	8	Š	
100 m deep)									
Pavilion Lake ^{¶¶}	3		0.01	0.5	<u>8</u>	Yes	8	°N	0.05
Ryan Lake##	3.5				Yes	Yes	8	Yes	
Lake Simcoe***				1.7	<u>8</u>	Yes	8	°N	0.01
Lake Sunapee†††	1.8				⁸	Yes	<u>8</u>	°Z	0.1

(1996). **Farmer (1975), Matthews and Heaney (1987), Mironov et al. (2002). ***Secretial et al. (2005), Farmer (1975), Matthews and Heaney (1987), Mironov et al. (2002). ***Secretial et al. (2017), Yang et al. (2017). ***Secretial et al. (2017), Yang et al. (2017). ***Secretial et al. (2017), Yang et al. (2017). ***Secretial et al. (2018). ***Secretial et al. (2017). ***Secretial et al. (2018). ***Secretial et al. (201 Barnes and Hobbie (1960) and Mironov et al. (2002). †This study.*Cortés et al. (2017). *Pieters and Lawrence (2009). "Bengtsson et al. (1996), Malm et al. (1997, 1998), Malm **Matthews and Heaney (1987). **Vehmaa and Salonen (2009), Jakkila et al. (2009), Kirillin et al. (2012), Salonen et al. (2014). **Bengtsson and Svensson (1996), Bengtsson et al. (1998), Mironov et al. (2002), Jonas et al. (2003), Petrov et al. (2006), Kirillin and Terzhevik (2011), Zdorovennov et al. (2013). "Malm et al. (1997). "Bouffard et al. (2016, 2019). lengths in Malm et al. (1997). than these, and their implications during winter will be developed in another paper.

In the following, we describe the meteorological conditions and changes in stratification under the ice in both lakes (Figs. 3–7). Our initial emphasis is on L. N2 in 2014. With the multiple arrays under the ice in that year, we address whether processes occurring in one or two dimensions contributed to heating of the lake. Processes analyzed include direct solar heating, internal waves, horizontal convection, and

penetrative convection. The detailed analysis for L. N2 facilitates interpretation of the data from the following year and from L. E1. Variability in density structure was induced by the between-year differences in temperature below the ice, the depth of the temperature maximum, and chemical stratification. When combined with differences in basin shape and rate of heating in spring, a suite of hydrodynamic processes occurred in both lakes, which modulated the transport of heat and solutes.

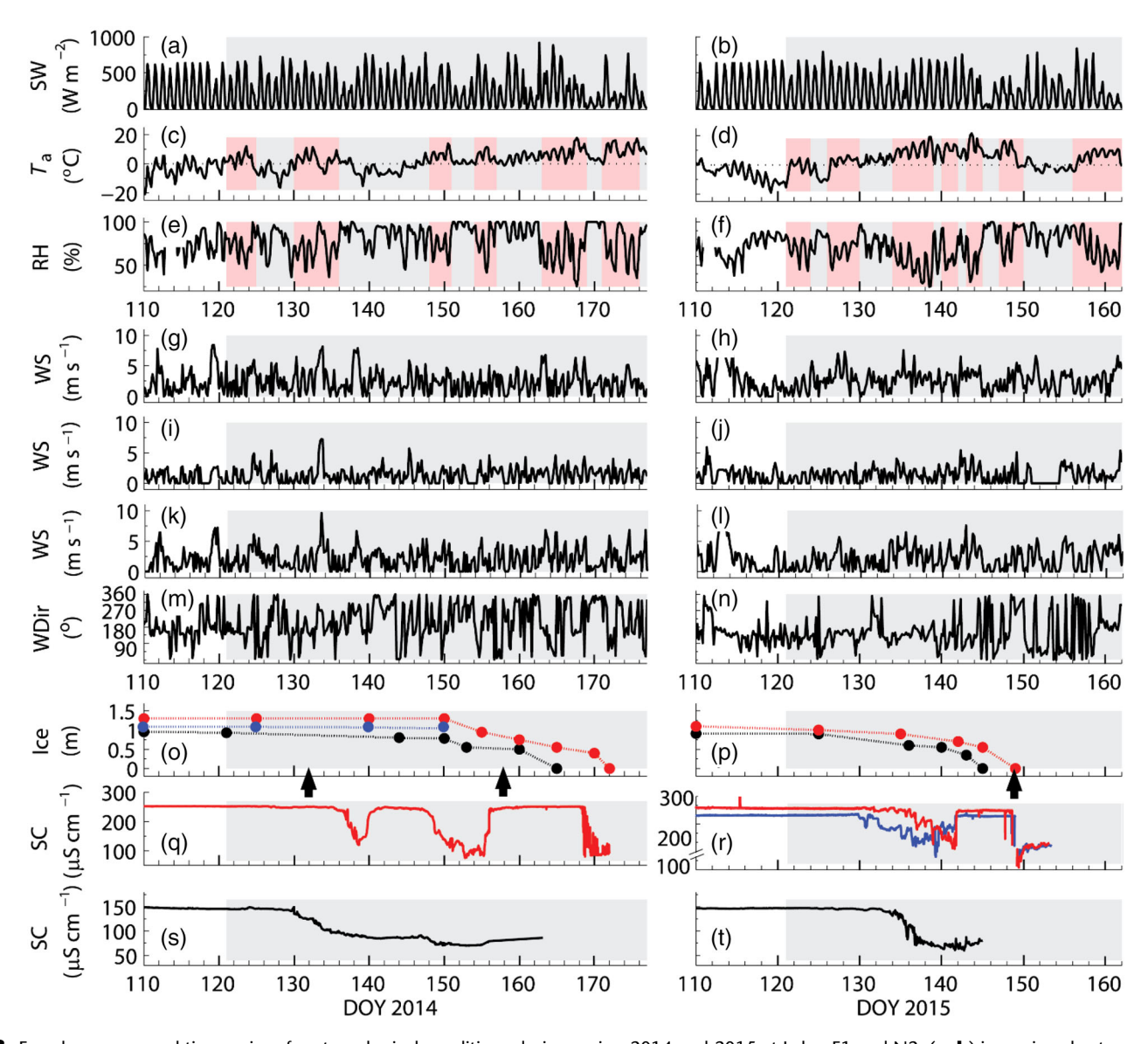


Fig. 3. Four-hour averaged time series of meteorological conditions during spring 2014 and 2015 at Lakes E1 and N2: (**a, b**) incoming short wave radiation, SW; (**c, d**) air temperature, T_a ; (**e, f**) relative humidity, RH; (**g, h**) wind speed, WS, at L. N2 north-west station; (**i, j**) wind speed at L. N2 south-east station; (**k, l**) wind speed at L. E1; (**m, n**) wind direction, WDir; (**o, p**) ice thickness from in-situ measurements and inferred from in-ice arrays, Ice, in L. N2 at the deep site (red) and L. E1 (black) in both years, and L. N2 at the shallow site (blue) in 2014 when thickness differed between sites (\sim 0.3 m), but not in 2015 (\sim 0.1 m), black arrows mark days when precipitation exceeded 2 mm; (**q, r**) specific conductivity at 1.75 m, SC, in L. N2 with array near T-02 (red) and T-03 (blue); (**s, t**) SC in L. E1 near the deep basin in 2014 and in the shallow basin in 2015. Incoming SW and precipitation are from the meteorological station at Toolik Lake and the other meteorological data from the L. N2 northwest station unless otherwise indicated. Gray shading marks warming periods when $T_a \geq 0^{\circ}$ C, and light red shading marks intervals with $T_a > 5^{\circ}$ C and RH < 60%.

Meteorological conditions, snow and ice thickness, and changes in specific conductance under the ice

Spring 2014 was characterized by a 6-week warming period with intermittent warming and cooling whereas warming was

persistent and lasted only 3 weeks before ice-off in 2015 (Fig. 3). The variable meteorological conditions in 2014 led to a later ice-off. Warming began in early May (~doy 130) in both years (Fig. 3c,d). Frontal activity was greater in 2014 with transitions

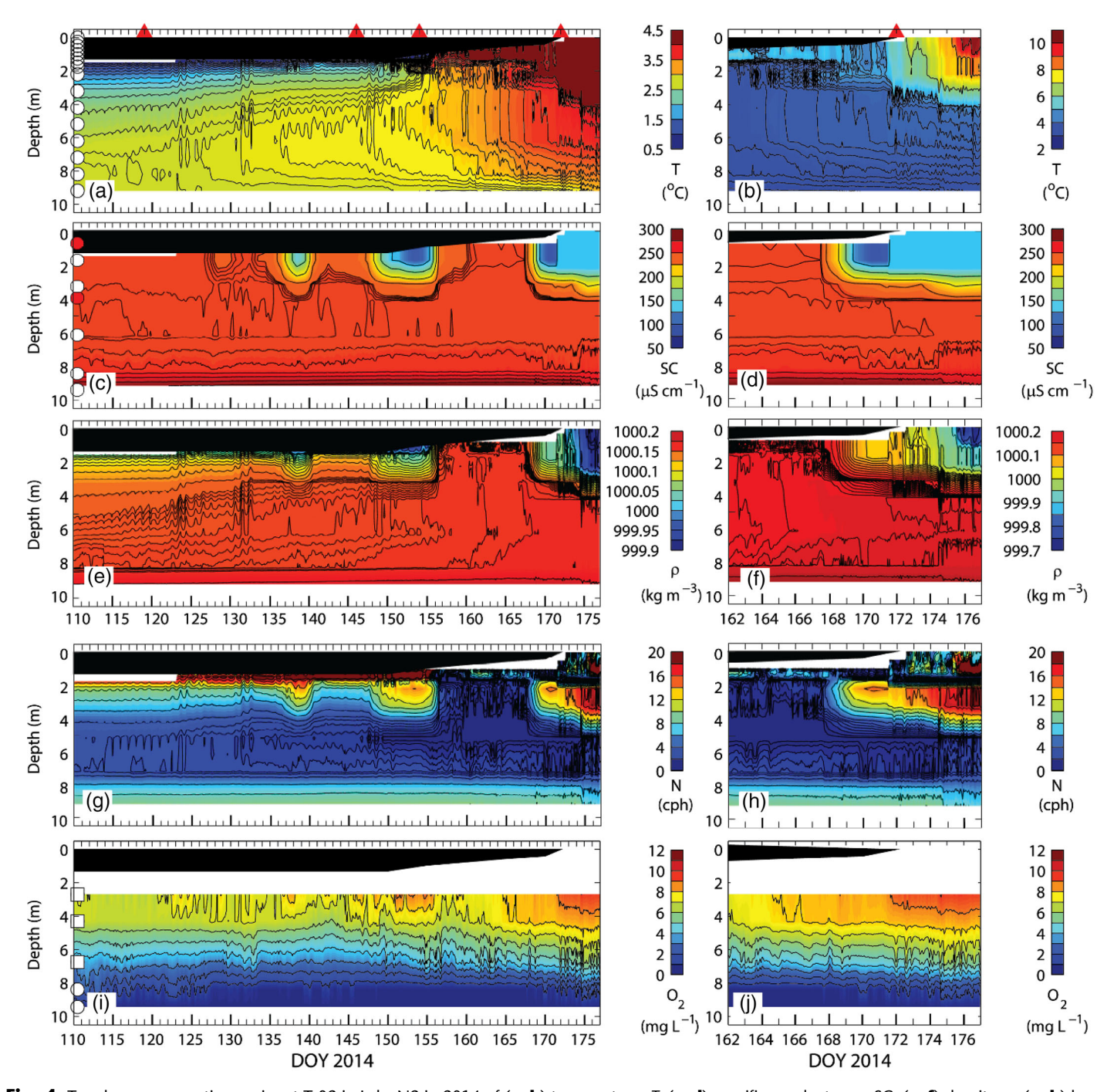


Fig. 4. Two-hour average time series at T-02 in Lake N2 in 2014 of ($\bf a$, $\bf b$) temperature, T; ($\bf c$, $\bf d$) specific conductance, SC; ($\bf e$, $\bf f$) density, ρ ; ($\bf g$, $\bf h$) buoyancy frequency, N, in cycles per hour (cph), with maximum value 22 cph; and ($\bf i$, $\bf j$) dissolved oxygen concentration (O_2). Panels to the right expand the period near ice-off. White dots mark depths of the loggers; red dots in ($\bf c$) apply to the period after ice-off with time series generated based on the CTD profile at that time and the time series of SC at 1.75 m. Oxygen contours in ($\bf i$) and ($\bf j$) use data below 8 m from T-02 and from T-03 above 6 m (white squares). Red triangles on top of $\bf T$ time series show dates when profiles were taken. Black in upper portion of panels indicates ice thickness. White space indicates no data.

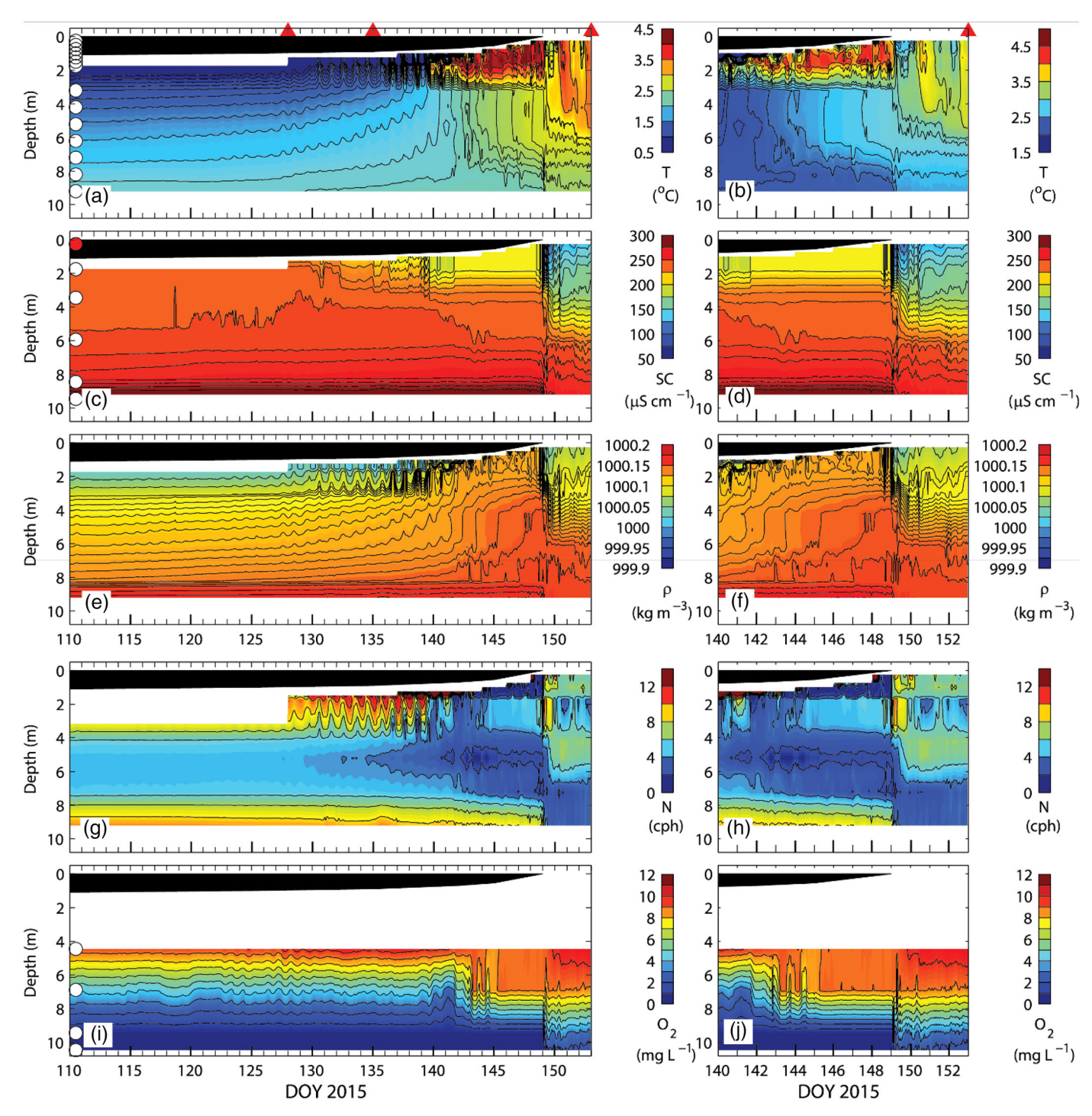


Fig. 5. As Fig. 4 except for Lake N2 in 2015.

marked by increases in wind speeds, and events with snowfall persisted (Fig. 3g,i,k). Warmer air temperatures and lower relative humidity marked the periods with southerly winds. In 2015, a stationary high prevailed over the region for several weeks. Consequently, air temperatures were consistently above freezing and relative humidity tended to be below 60% from ~doy 125 to 145. Winds tended to be southerly and were

persistently elevated during the warming period, with these combined conditions conducive to loss of snow cover on the ice. Additionally, snow cover on the landscape was less in 2015 than in 2014 (Cortés et al. 2017). Ice thickness tended to be ~ 1 m in both lakes in both years with the exception being the more exposed western side of L. N2 in 2014 where it was ~ 1.5 m. Decreases in ice thickness occurred with increased air

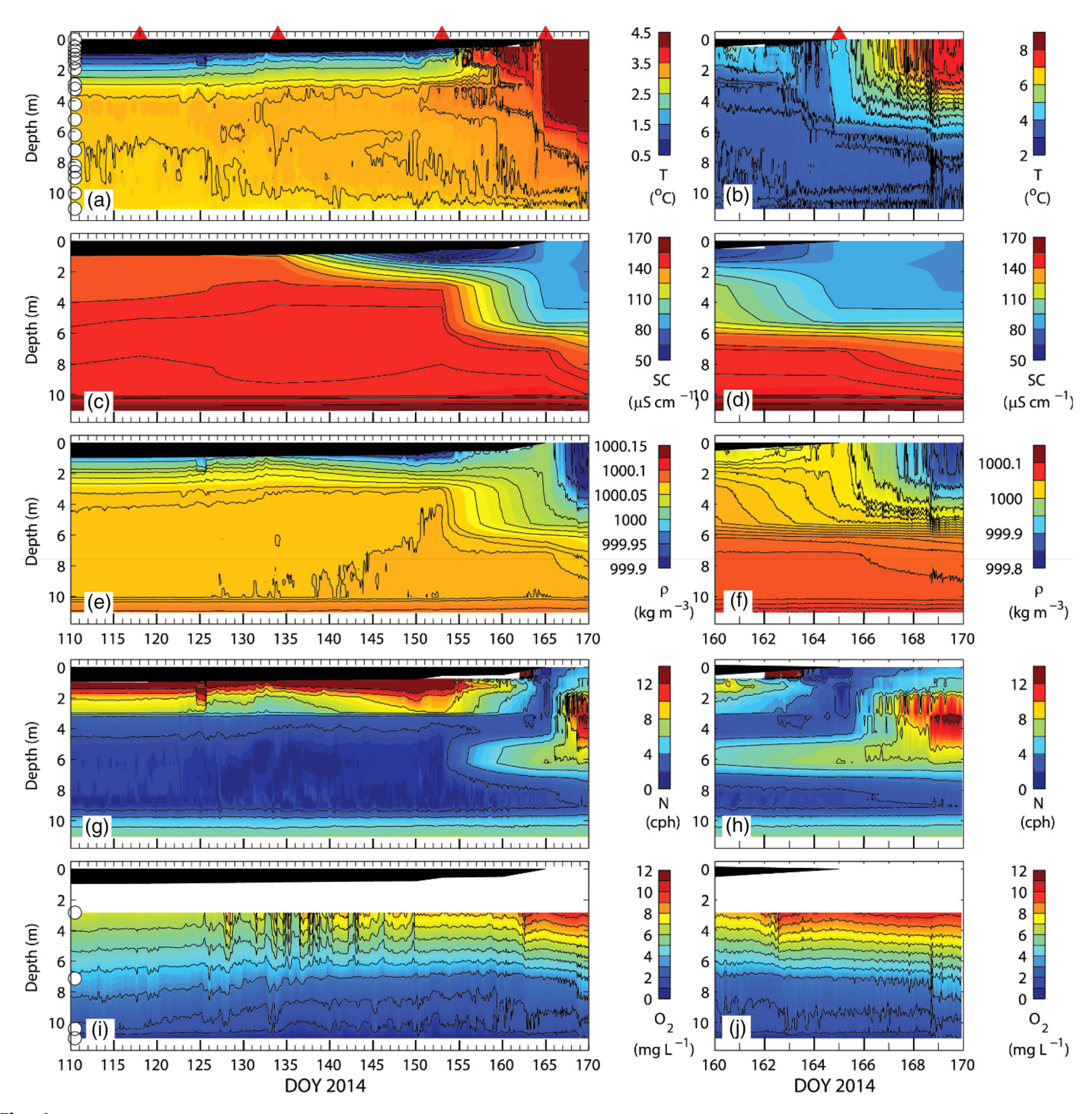


Fig. 6. As Fig. 4 except for Lake E1 in 2014. The time series of SC was computed with data from CTD profiles (dates indicated by red triangles) including profiles taken before and after the period shown.

temperatures, reduced relative humidity, and sustained winds (Fig. 3c–p). Measurements of snow depth on the lakes were intermittent with values ranging from 0.1 to 0.3 m when snow was present; thickness was greater on the eastern sides of both lakes. The lower wind speeds at the southeast meteorological station relative to those measured to the northwest are

indicative of the sheltering from wind to the southeast which would have led to the greater snow cover and thinner ice to the east on L. N2 in 2014 (Fig. 3o).

Decreased values of SC in the in-ice arrays indicated the presence of snowmelt and, near ice-off, the freshening of the upper water column by ice melt (Fig. 3q-t). The decreases occurred

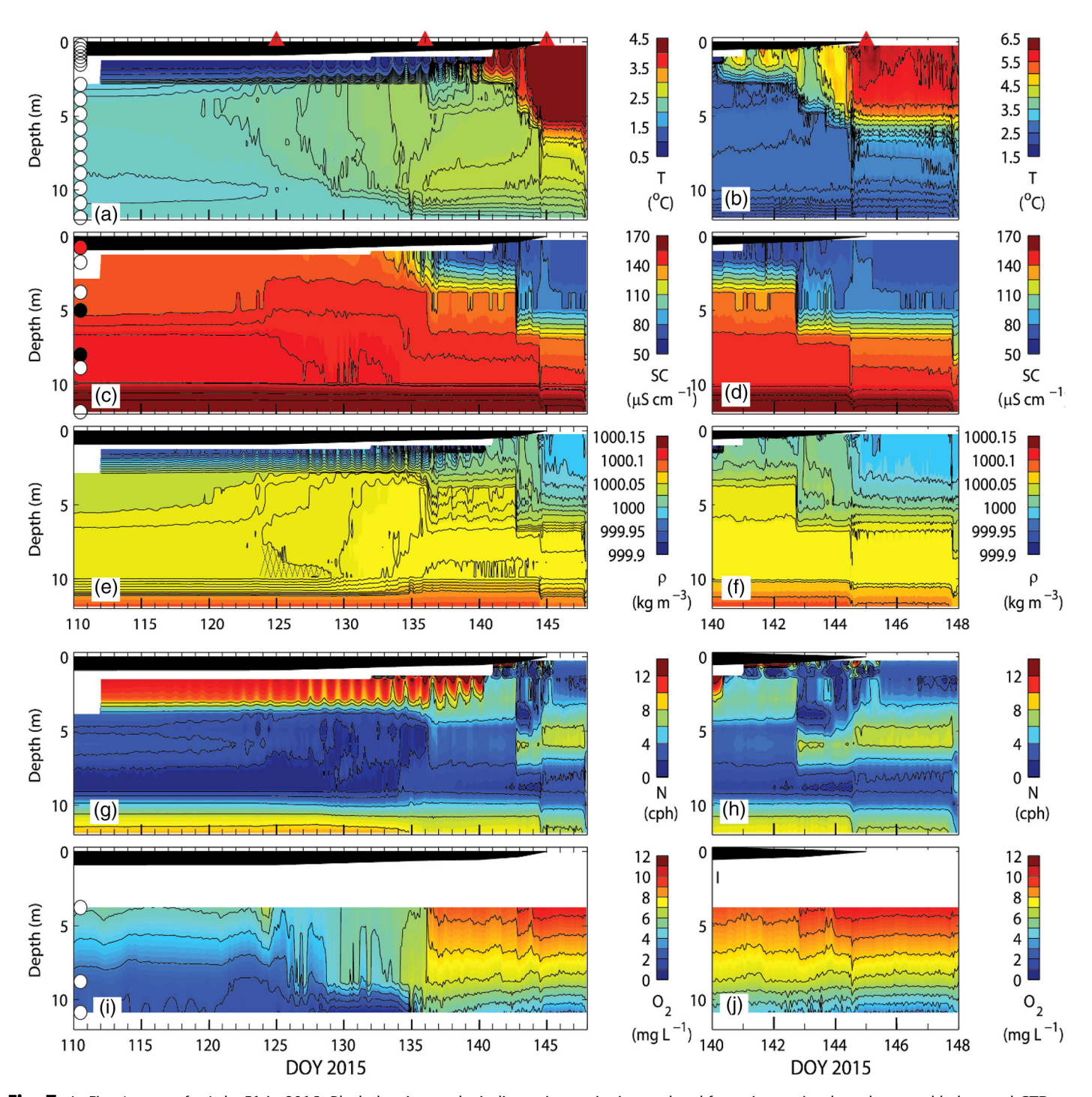


Fig. 7. As Fig. 4 except for Lake E1 in 2015. Black dots in panel c indicate time series interpolated from time series data above and below and CTD profile data. Hatching in panel e indicates uncertainty in density due to insufficient SC sensors mid-water column.

either during or immediately after periods with increased air temperatures. The initial decreases in L. N2 were followed by a return to the initial values, indicating snowmelt entered and exited the lake. The final decreases persisted through ice-off suggesting the water was a combination of snowmelt and ice melt. The decreases in 2015 were less than those in 2014, as expected with less snow in 2015. Minimum values occurred at T-03, closer to the inlet, on

day 136 and similar minimum values occurred at T-02, 100 m distant, on day 142, indicating slow flow across L. N2. In L. E1, after initial freshening, SC remained lower than the initial values until ice-off indicating snowmelt persisted in the lake. The slight increases in SC toward ice-off imply mixing with lake water with its higher SC. Incoming snowmelt induced a near-surface chemocline, with the maximum difference in SC during freshening

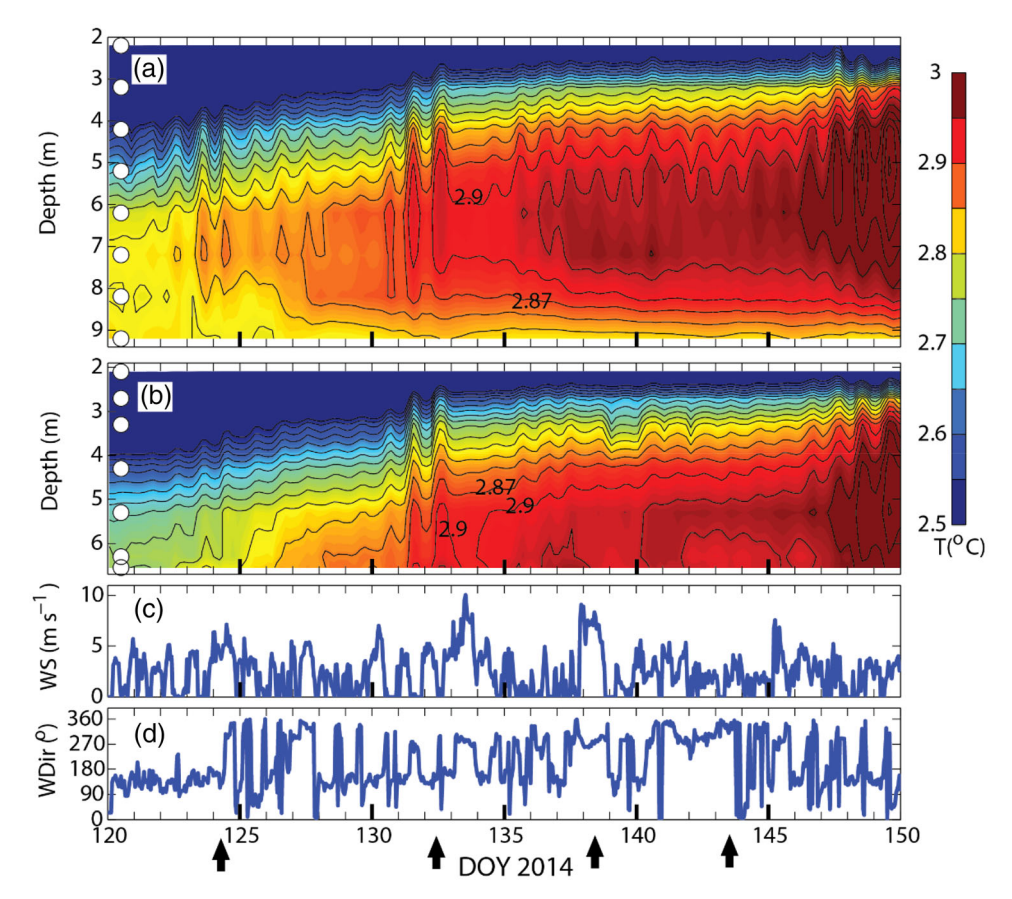


Fig. 8. Four-hour averaged temperature contours at (a) T-02, (b) T-03, (c) wind speed, and (d) direction for doys 120–150 in L. N2 in 2014.

relative to the initial near-surface concentration 180 μ S cm⁻¹ in L. N2 and ~ 120 μ S cm⁻¹ in L. E1.

Ice-off occurred on doys 165 and 145 (14 June 2014 and 25 May 2015) in L. E1 and 172 and 149 (21 June 2014 and 29 May 2015) in L. N2. Low sun angles combined with greater sheltering from the south led to the later ice-off dates in L. N2. Air temperatures were above freezing point for at least several days after ice-off in 2014 and at L. E1 in 2015 whereas they were below freezing following ice-off at L. N2 in 2015.

Stratification under the ice in L. N2 in 2014

The distribution of temperature and specific conductance changed over time (Fig. 4). The warmest water was initially near the bottom but a temperature maxima began to develop by doy 120 at 7 m with density stabilized by slight increases in SC below. The chemocline began at 8 m. In early spring, diel heating and cooling was prevalent as indicated by the daily rise and fall of isotherms with slow heating of the water column (Figs. 4 and 8). Regions of near-isothermy developed where temperatures were warmest beginning by day 120 (Fig. 4). However, these regions did not progressively deepen over time as expected with RDC. Instead, they rose vertically and were always associated with temperature maxima. Our instrument arrays indicated that SC increased at 8 m and below and that the SC minimum persisted

near 6 m. Thus, the rise in the temperature maximum and increases in SC in the lower water indicate density stratification was maintained in the lower water column that precluded deepening by RDC (Fig. 4).

Mid-water column expansions and contractions

Unsteady winds were a prevalent feature throughout the study including the initial period of warming (Figs. 3, 8, and 9). The diurnal expansions and contractions on doys 122–123 initially occurred when winds were southeasterly with speeds dropping below anemometer threshold in the day and increasing at night. Southeasterly winds would cause downwelling at night at T-02 and T-03 followed by upwelling on relaxation in the day. The isotherms at both stations illustrate this pattern. Winds increased and shifted to westerly on doy 124. Upwelling of cooler water occurred below the warm layer at T-02 and an abrupt upwelling of warmer water occurred at the shallower T-03 (Fig. 8). Winds shifted to northerly later in the day. Upwelling continued at T-02 (Fig. 8).

Second vertical mode internal wave motions were prevalent at other times (Fig. 8 and Fig. S1). Diel expansions and contractions occurred during periods with daytime lulls in the wind and nighttime increases (e.g., doys 130–133, Fig. 8). At times, these led to larger increases in temperature near the

bottom at T-03 than expected from direct solar heating, providing further support for upwelling at that site (Fig. S2, doy 131). Larger scale contractions and expansions occurred in response to strong westerlies. Contraction of the 2.9°C isotherm occurred at T-03 in response to the 7 m s⁻¹ westerly winds on doy 134. The upwelling below 7 m persisted for several days at T-02. Downwelling of the 2.9°C isotherm also occurred at T-03 in response to the strong wind, followed by its upwelling as the wind relaxed. Downwelling also occurred at T-03 in response to the increased winds on doy 138 with a more muted upwelling response at T-02. When winds were northerly, upwelling occurred in the lower water column at both stations. Such can be observed in response to the northerlies on doy 134 and the more persistent northerlies starting on day 143. The currents associated with the wind-induced expansions and contractions are expected to cause horizontal flow of water and transport heat within the lake.

While it is tempting to speculate that the increase in temperature in the center of the expansions would have induced convective mixing, in fact these features occur at depths with a minimum in SC (Figs. 2 and 4). Hence, with the change in density as a function of temperature decreasing as temperature approaches 4°C and with SC increasing below the warmer water, it is not clear that mixing by RDC occurred as a result of the apparent instability. In fact, temperature fluctuations occur in the heated regions as well as above and below in response to changes in wind velocity. These are often in phase in the raw temperature data indicating high-frequency waves have been generated. Since the motions tend to be coherent, they are not indicative of turbulence. Thus, the warming in the center is more likely indicative of warmer water, likely from the west where snow cover had been less, being advected on expansion of the 2nd vertical mode waves. The near isothermy at night, then, results as the waves contract and warmer water is advected laterally. When the changes in temperature are viewed in the context of internal waves, and given that the heating over diel cycles is often relatively close to that expected by direct solar radiation or has been moderated by upwelling, as at T-03 at 6.6 m on doy 131 (Fig. S2), convective mixing may have contributed to the nearisothermal regions but there is no evidence for RDC.

Intrusions at the base of the mixed layer

Abrupt increases in temperature occurred at the base of the warm layer beginning on day 153 at T-03 and on doy 158 at T-02 (Fig. S1 and Fig. 9). Just prior to these events, shallow regions to the west and east began to warm more rapidly possibly due to moating, as observed by doy 154, and resultant increased penetration of solar radiation, by sediments warming the overlying water at night due to their gaining heat in the day (Zdorovennova 2009), and warmer incoming snowmelt (Fig. 9d,g). Downslope flows are expected when warming is greater at nearshore sites. However, the incoming snowmelt also freshened the upper water column to at least

2 m depth (Fig. 3q), and changes in temperature were less than predicted from solar heating over diel cycles at 4 m and occasionally at 5 m for several days prior to these events (data not shown), implying that freshening may have occurred to those depths as well. The deep warming events occurred as northerly winds dropped to zero. With our stations along the centerline of the basin relative to northerly winds, the upwelling and downwelling would not be appreciable there. However, the movements may have entrained water from shallow areas, which had not been influenced by fresher snowmelt, which then flowed offshore on cessation of the upwelling to the north.

Effects of snowmelt and melting ice on near-surface stratification

The cold, fresher snowmelt initially intensified the density gradient between 2 and 4 m creating a pycnocline. Snowmelt flowed in and out of L. N2 in 2014, which led to intermittent strong density contrasts (Fig. 4e). Overtime, the pycnocline broadened (Figs. 4a,e). This pattern also occurred in the other lakes (Figs. 5a,e, 6a,e, and 7a,e). As the ice thinned in the week prior to ice-off, temperatures between the ice and the pycnocline increased to between 4°C and 4.5°C further decreasing the density difference between the upper fresher layer and the water below such that N was reduced. However, the chemocline persisted separating the upper, fresher layer from the water below. The upper layer underwent diel heating and cooling independently of the water below. Before ice-off, N within the upper, fresher layer was less than 4 cph. Between the snowmelt induced pycnocline and the near-bottom pynocline, the near-isothermal layer was 3 m thick. It did not deepen before ice-off, indicating RDC did not occur.

Processes causing warming and transport of heat

Direct solar heating explained the warming at depth on many days with departures when winds were elevated causing upwelling or downwelling. Internal wave motions that advected warm water to and from the measurement sites provide an explanation for near isothermy at night before the ice thinned. Increasing solutes in the lower water column precluded RDC despite the mid-water column temperature maxima. Inflows of warmer water thickened the near-isothermal region before ice-off and deepening by penetrative convection was not observed (Fig. 9). In fact, near-isothermy only persisted for about 3 h each night. Slight increases in SC with depth within the near-isothermal region may have restricted RDC. SC increased by 3 μ S between 3.3 and 6.3 m. In fact, when temperatures are just below 4°C, as here, a 1 μ S increase in SC over a 1 m interval stabilizes the density stratification relative to instabilities induced by overlying water's being 0.05°C warmer, as occurred with diurnal heating. Thus, rather than RDC being an important process, direct solar heating attributed for most of the warming at depth with internal waves redistributing heat. Horizontal convection induced by

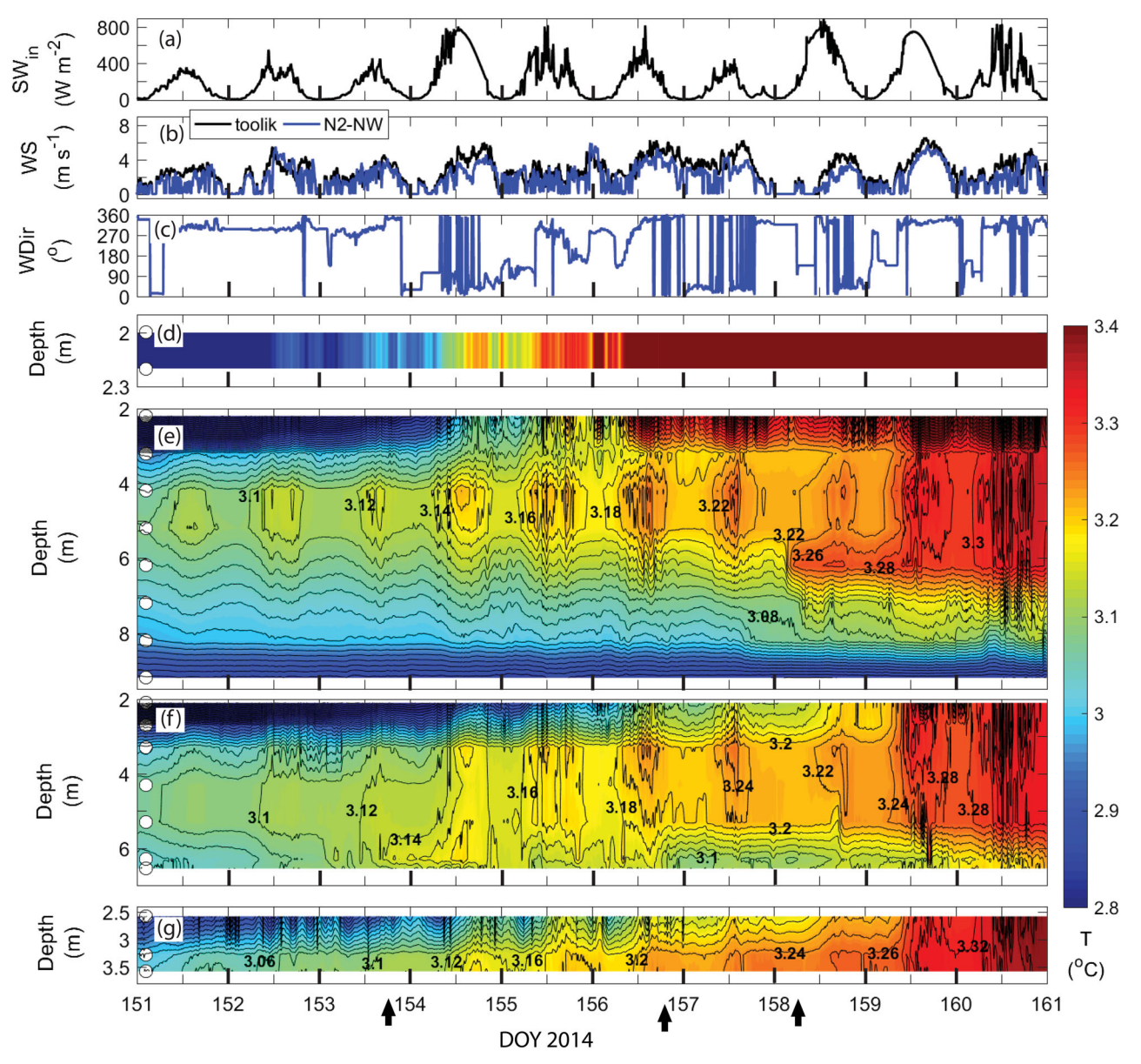


Fig. 9. Five-minute (**a**) incoming short-wave radiation (SW_{in}) at Toolik Field Station (TFS, black), (**b**) wind speed (WS) at TFS and L. N2 north-west station (blue), and (**c**) wind direction (WDir) at L. N2 north-west station. Thirty-second isotherms every 0.02° C at (**d**) T-01, (**e**) T-02, (**f**) T-03, and (**g**) T-04 for doy 145–155 in L. N2 in 2014. Some of the isotherm values are marked. Intrusions of warm water formed in depth at T-03 due to horizontal transport when the moat formed on ~day 154. After that day, water on the western end (T-01) started to warm quickly until it intruded at 6 m at T-02 on day 158 when wind relaxed and changed to southerly. That wind shift would have contributed to the downslope flow of warmer water with still relatively high SC from T-01 to T-02. Upwelling of colder water at depth at T-03 occurred late on day 156 during the contraction of a 2nd vertical mode wave. Arrows mark the features described.

warmer nearshore water may have contributed to warming deeper in the water column. Results from L. N2 in 2014 will thus help with interpretation of time series data from the other lakes in our study.

Stratification in L. N2 in 2015

The colder temperatures in early spring in L. N2 in 2015 combined with steady increases in temperature with depth and increased SC below 6 m meant that stratification over the

water column was strongest below the ice in that lake in that year (Figs. 4g, 5g, 6g, and 7g). Castaway profiles obtained at stations to the east and west in late March and late April indicate that downward mixing of cryoconcentrated salts had occurred as in 2014 (Fig. 2) and that the minimum in SC deepened from 3.5 to 4.5 m as the ice continued to thicken (data not shown). As for N2 in 2014, the measured change in temperature was often equal to the computed change based on incoming solar radiation, indicating that solar heating caused

the changes in temperature. By doy 128 when snowmelt increased, the change in temperature at 4 m was initially less than predicted from incoming solar although on, for example, doys 134 and 136, it was sometimes higher. Thus, snowmelt influenced temperatures in the upper 4 m. With warming in spring, the temperature differences and density differences between depths decreased (Fig. 5). Comparison of time series data from multiple stations as for 2014 indicate that internal

waves were prevalent over the spring and that horizontal flows of warmer water occurred which contributed to the reduction in density difference toward the end of spring. Eventually, isopycnals were vertical between the near-surface pycnoline from snowmelt and the near-bottom pycnocline from chemical stratification. Thus, the buoyancy frequency N decreased mid-water column. However, intrusions of warmer water occurred during the final period before ice-off

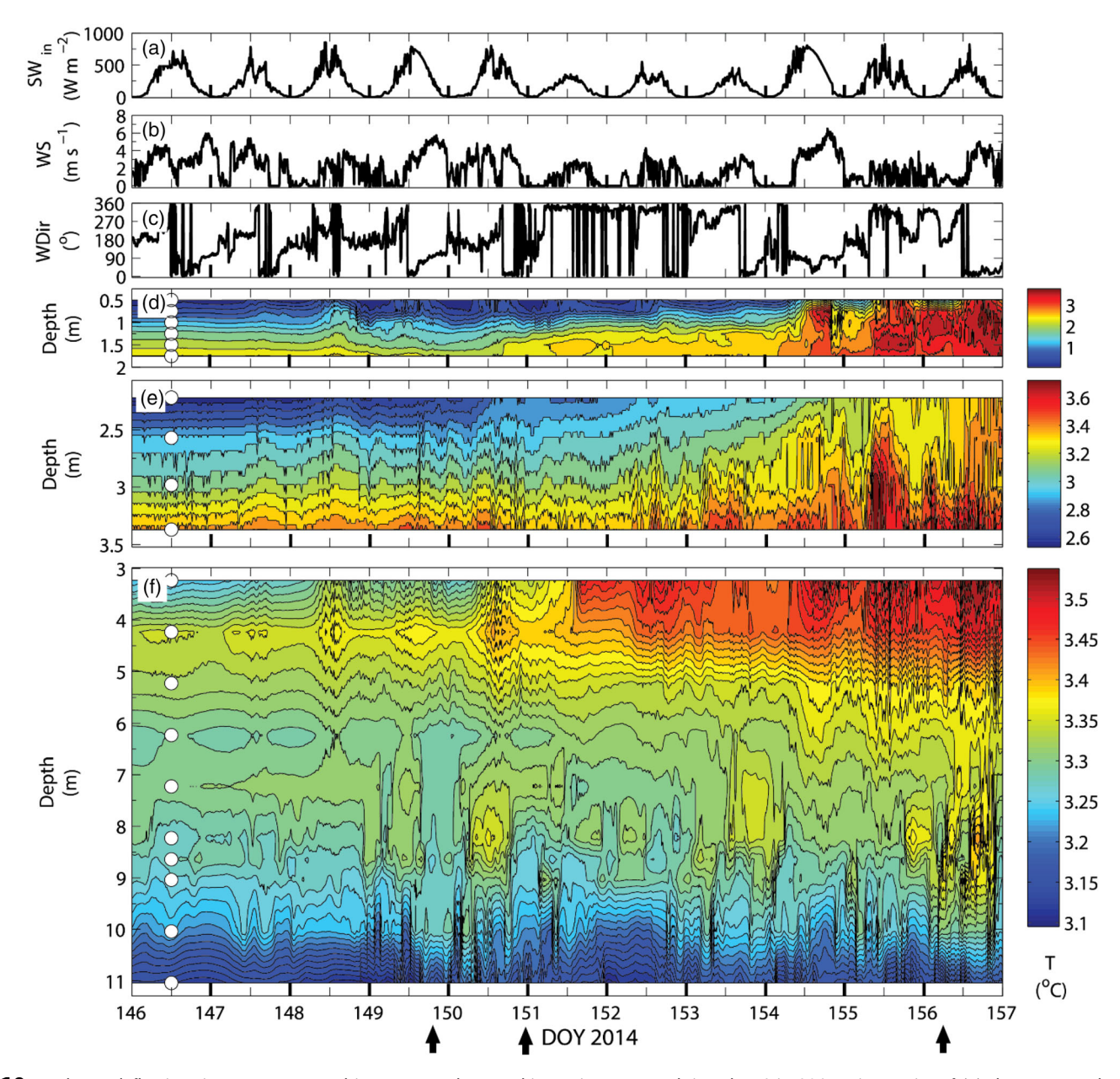


Fig. 10. Isotherm deflections in response to ambient meteorology and incoming snowmelt in Lake E1 in 2014. Time series of (a) short-wave solar radiation, SWin; (b) wind speed, WS; (c) wind direction, WDir; (d) isotherms in the upper 2 m from the in-ice t-chains; (e) isotherms in the shallow basin, T-01; and (f) isotherms below 3 m in the deep basin, T-02. White dots mark depths of the loggers. An increase in incoming snowmelt can be seen beginning on doy 148 as temperatures under the ice become colder and the volume of cold water increases (d). Arrow on doy 149 marks 2nd vertical mode expansion from 4 to 11 m in response to the incoming snowmelt or wind. Arrow on doy 156 marks distortion by internal wave motions of an intrusion of warmer water. Arrow on doy 151 marks transition when snowmelt moderated water temperatures above 4 m more than incoming solar.

indicating that not all the temperature increase at T-02 that would have led to instabilities and caused convection was from direct solar radiation. Although isothermy occurred at night between the two pycnoclines, the mixing region did not deepen. Hence, RDC was not occurring.

Stratification in L. E1 in 2014

The patterns in L. E1 differed from those in L. N2 due to weaker stratification mid-water column, the presence of midwater column temperature maxima, increases in SC below the temperature maxima, and greater freshening of the upper water column by snowmelt (Figs. 2, and 4-7). The shallower temperature maxima in L. E1 meant that temperatures initially warmed from 4 m downward in both years (Figs. 6 and 7). Stratification below 4 m was weak with N < 4 cph. However, the density stratification was such that in early spring 2014, diurnal heating and cooling occurred in the more stratified layer centered at 4 m (Fig. 10). The weakly stratified layer below 6 m and above the chemocline had interleaving layers of warmer and cooler water. These are in part stabilized by differences in SC, although profile data indicate instabilities that would cause mixing (Fig. 2f). By day 151, the density gradient above 4 m had been strengthened by incoming snowmelt. The thermal stratification in the day became stably stratified. Below 5 m, diurnal heating and nocturnal cooling occurred with a slow warming of the lower water column (Fig. 10). The boluses of warmer water, as at 8 m on day 150, are likely indicative of intrusions. In the last five days before ice-off, gradients in SC persisted and were stronger above 5 m. Although temperature differences were less than 0.1°C between 5 and 9 m, high-resolution contours had a similar appearance to those in Fig. 10, implying that weak chemical stratification had enabled persistent density stratification, despite minimal temperature differences, such that an internal wave field was sustained and intrusions of warmer water continued. With the persistent chemical stratification, RDC did not occur.

Heat budgets in L. E1 in 2014

Incoming snowmelt and the freshening of the upper water column moderated the mixing dynamics in L. E1 at deeper depths than in L. N2 (Fig. 10). We assumed an albedo of 0.5 and verified it by equality of Q_S and Q_T below 4 m on a sunny day following a windy one. Incoming irradiance was insufficient to induce warming below 7 or 8 m. Initially, the warming that occurred in the day and cooling at night had a maximum at 4 m as incoming heat was trapped due to the extra stability enabled by a slight increase in specific conductance. On doy 149, more heat was lost at night at 2 and 3 m than gained in the day, due to the inflow of cold snowmelt. On day 151, temperatures increased at 3 m. The computed heat increase exceeded that expected from solar radiation, and thus indicates inflows of warmer water. CTD profiles indicate that fresher water from snowmelt had penetrated from 2 to 4 m by this date. Thus, an upper layer was created with diel heating and cooling which at times led to isothermy. Q_S often exceeded Q_T from 3 to 5 m from doy 149 until doy 157 on days when $Q_T = Q_S$ at depths below. The upper water column was cooled more by incoming snowmelt than heated by solar radiation. Heat budgets over diel cycles below 5 m were confounded by the internal waves and intrusions to be further discussed below. It was clear that Q_T exceeded Q_S in the bottom pycnocline.

Internal waves in the lower water column of L. E1 in 2014

Upwelling and downwelling occurred below the density gradient at 4 m and pronounced oscillations occurred in the bottom meter and a half in L. E1 in 2014 (Fig. 10). The internal wave field was more complex in L. E1 than that in L. N2 was in 2014. At times, 2nd vertical mode internal waves are apparent, as on day 149 and from day 151 to 153. There were also expansions and contractions within the near-bottom pycnocline, which appear to be independent of the overlying motions. The near-bottom downwelling beginning early on day 149 with upwelling by mid-day on day 150 may be a response to increased inputs of snowmelt (Figs. 3 and 10d,f). However, wind speed increased to 6 m s⁻¹ and downwelling was largest when wind speeds were highest. Upwelling occurred near midnight on day 151 when winds ceased. Thus, the internal waves appear wind driven. The boluses of warm water, as in L. N2 in 2014, appear to be intrusions from shallower depths, especially as their frequency increased over time. Unlike observations in other studies (Farmer 1975; Bouffard et al. 2016), the internal waves were not driven by penetrative convection. The increase in heat content in the bottom pycnocline relative to that expected from solar heating is indicative of the downward movement of heat. The heating resulted from the intrusions and the internal wave induced mixing.

Stratification in L. E1 in 2015

Stratification dynamics differed in L. E1 in 2015 due to a more rapid increase in snowmelt (Figs. 3 and 7; Figs. S3 and S4). Similar to conditions in 2014, the temperature maximum was initially at 4 m and temperatures below progressively warmed. With the initial weak stratification below the temperature maximum, computed isopycnals indicate upwelling and downwelling presumably from internal waves. As heating increased, the amplitudes decreased. Diurnal heating followed by nearisothermy at night occurred between 3 and 4 m by doy 120. However, as with L. N2, wind direction varied such that the near-isothermy is not necessarily indicative of convection. From doy 124 to 128, the largest increases in temperature occurred at 6 m and usually at night (Fig. S3). This heating, as in 2014, was likely caused by downslope currents from shallow nearshore regions. By doy 129, incoming snowmelt freshened the upper water column. The water column stratified to 5 m in the day with warmer temperatures above cooler (Fig. 11 and Fig. S4). As in 2014, this stable temperature stratification was possible due to the stabilizing effect of the decrease in SC from the surface downward. Heat was lost at night. The layer acted similarly to

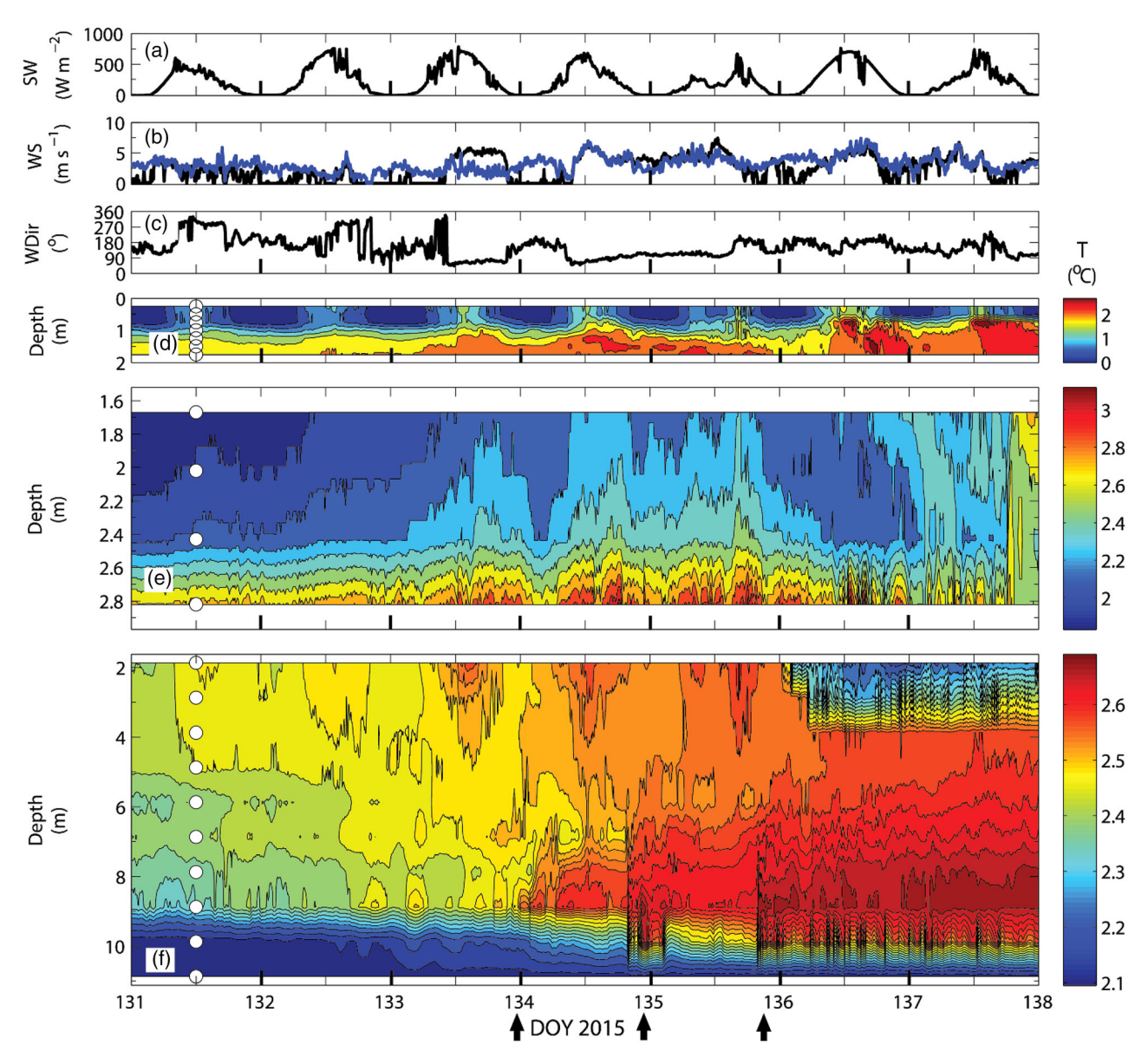


Fig. 11. Time series in Lake E1 in 2015 of (**a**) shortwave radiation, SW_{in}; (**b**) wind speed at L. E1 (black) and Toolik Lake (blue), WS; (**c**) wind direction, WDir; (**d**) isotherms in the upper 2 m from the in-ice t-chains, in the shallow basin; (**e**) isotherms in the shallow, western basin, T-01; and (**f**) isotherms below 3 m in the deep basin, T-02. White dots mark depths of the loggers. Diurnal mixed layer stabilized by freshening from snowmelt with intermittent gravitational intrusions from nearshore heating below through doy 136 (f; and see Fig. S3). Warming of the lower water column from snowmelt induced gravity currents (see Fig. 12).

mixed layers found at temperatures above 4°C, and, in fact, supported an internal wave field in part energized by changes in wind direction (Fig. S4). A thermocline occurred at 5 m and below it, on days 129 to 134, the water was weakly stratified with intermittent intrusions of sometimes cooler and sometimes warmer water initially between the chemocline and 8 m and subsequently to 7 m (Fig. 11 and Fig. S4). The intrusions may have been from downslope flow or may have resulted from the spatial variability of temperature and specific conductance as noted in Castaway profiles (data not shown). The periodicity of the intrusions, however, was, in part, coincident with changes in wind speed and direction implying their movement may

have been abetted by internal wave motions. Within the lower water column, isotherms upwelled and downwelled and eventually deepened further and contributed to warming of the deeper pycnocline. More sustained winds contributed to deepening of the stably stratified mixed layer beginning on day 132 with this effect particularly noticeable on day 134 when it eroded the thermocline at 5 m (Fig. 11 and Fig. S4).

Additional changes occurred in the lower water column beginning on day 134. These were coincident with increased snowmelt (Fig. 3). Temperature increased between 8 and 9 m beginning early on doy 134 with further increases later on doy 134 and late on doy 135 (Fig. 11). These changes co-occurred with changes in

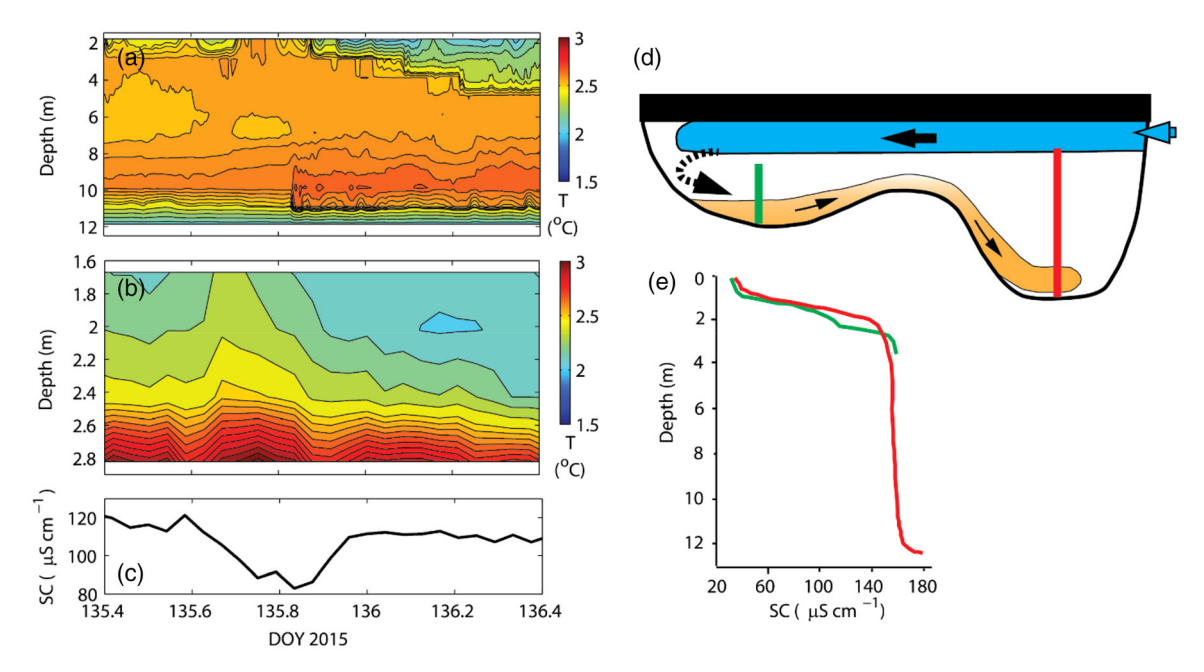


Fig. 12. Influence of snowmelt on the lower water column and benthic boundary layer in Lake E1 in 2015. (a) Temperature contours at deep station, T-02; (b) as in a, but for the shallow station, T-01; and (c) time series of specific conductivity (SC) at 1.75 m at T-01. (d) Inferred processes at onset of snowmelt: Incoming snowmelt plume (blue) displaces near-bottom water in the shallow basin such that it flows as a gravity current (orange) into the deeper basin at 10 m. Black overbar indicates ice; (e) profiles of SC in the deep and shallow station during snowmelt in 2013. Density of the near-bottom water in the shallow basin, based on measured temperature in 2015 and SC mid-water column at the deep station in 2015, as noted in paired CTD profiles from spring 2013, was 0.008 kg m⁻³ higher that at 10 m in the deep basin in 2015, supporting the inferred intrusive gravity current.

the shallow basin including cooling of surficial water and downwelling of cooler water below 2.5 m (Fig. 11e). The abrupt change late on day 135 occurred with considerable cooling of the shallow basin and additional decreases in SC at 1.75 m (Figs. 11f and 12c). The temperature of the now warmer water at 9 m was similar to that which had been found at depth in the shallow western basin. We infer that water from the western basin was displaced by incoming snowmelt. Because of its higher near-bottom temperature and relatively higher SC, the water initially at depth in this basin flowed downslope as a gravity current (Fig. 12). The successive arrivals of progressively warmer water imply that incoming gravity currents displaced the prior intrusions upward. From day 135 onward, the lower water column warmed, the buoyancy frequency increased mid water column, and the stratification supported an internal wave field (Fig. 11). Complex motions occurred in the bottom boundary layer in the deep basin of L. E1 in 2015 in response to the incoming gravity currents (Figs. 11 and 12). The near-bottom thermocline compressed with compression followed by temperature fluctuations indicative of internal waves. Stratification weakened within the near-bottom chemocline beginning on day 135 contributing to the increase in density of the overlying water (Fig. 7e,g). The warming and oxygenation of the pycnocline indicates mixing of incoming water with near-bottom water.

Oxygen under the ice

The oxygen depletion in the upper water column and hypoxia in the lower water column of both lakes is indicative of

respiration under the ice (Figs. 4-7, bottom panels). For example, at 3 to 4 m at all sites in L. N2 in 2015, concentrations were 6 mg L^{-1} and ~ 50% of saturation. The physical processes in spring contributed to oxygenation but did not alleviate near-bottom hypoxia except in L. E1 in 2015. The intrusions in L. N2 in 2014 transported oxygen to 6 m depth in the eastern part of the basin, and those in L. E1 in 2015 alleviated hypoxia in the lower water column (Figs. 7 and 11). Incoming snowmelt increased oxygen concentrations. During spring in L. N2 with incoming snowmelt, offshore values increased to 60% of saturation and near shore values to 80%. Oxygen penetrated more deeply near ice-off in L. N2 in spring 2015 than 2014. Thus, incoming snowmelt oxygenated the upper water column and downslope gravity currents locally oxygenated the water column above the chemocline. Hypoxia was only alleviated in the chemocline by the presumably more energetic gravity currents induced by snowmelt.

Mixing dynamics at ice-off

Temperature and density stratification persisted in the two lakes until ice-off in both years despite weakening stratification as the ice thinned (Figs. 4–7, right panels). In addition, the near-surface freshening from snowmelt and melting ice allowed the near-surface density gradient to persist even as temperatures in the upper layer warmed to 4° C and above. Hence, at ice-off, there were two pycnoclines, one closer to the surface and one near the bottom. The near-surface density gradients in L. N2 were centered at 3 m. That in 2014 was the strongest with N at

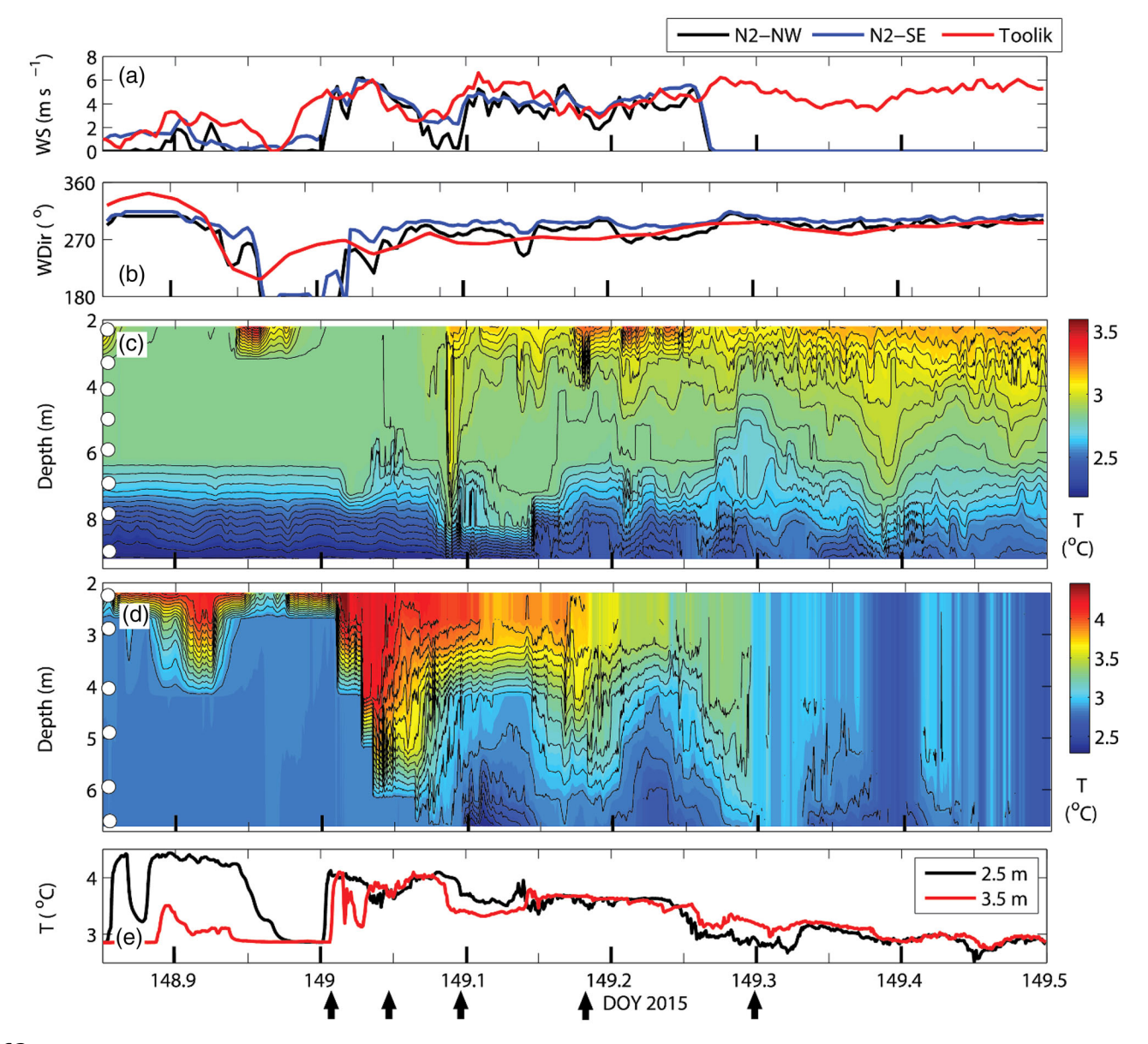


Fig. 13. Upwelling and downwelling at ice-off in Lake N2 in 2015. Time series of (**a**) wind speed (WS) and (**b**) wind direction (WDir) from N2-NW, N2-SE, and TFS meteorological stations; (**c**) isotherms at T-02; (**d**) isotherms at T-03; and (**e**) temperatures at 2.5 and 3.5 m at T-04. Meteorological data included from Toolik Lake as stations at L. N2 recorded zeros when air temperatures dropped to freezing and snowfall occurred during the cold front which began shortly after ice-off. Temperature stratification was stabilized by the increases in SC with depth (Fig. 4). Arrows mark events described in the text.

3 m exceeding 12 cph whereas in 2015 $N \approx 4$ cph. In contrast, in L. E1, N was ~ 5 cph and the pycnocline was centered at 6 m due to wind-induced events that deepened the upper layer prior to ice-off. Internal waves were prevalent on the upper density interface before ice-off, with their asymmetrical shape indicative of nonlinearity. In the following, we summarize the internal wave dynamics induced by wind acting on the surface of the water.

Wind induced mixing at ice-off

The winds at ice-off, typically 5 to 6 m s⁻¹, were sufficiently strong relative to stratification that Lake and

Wedderburn numbers, L_N and W, dropped to values near or below 1 in both lakes and in both years. The resulting mixing was evident by an abrupt descent of the thermocline, an increase in the gradient in SC, and an intensification of the density gradient mid-water column associated with heat being mixed into the lake and the freshening above the thermocline (Figs. 4–7, right panels). Attributes of the near-bottom pycnocline changed as well. The typical response was an abrupt increase in temperature, a decrease in SC, and a decrease in density and the density gradient such that the bottom pycnocline broadened. This pattern was observed in Lakes N2 and E1 in 2015; however, a

second event with low L_N was required to cause these changes in L. N2 in 2014. Dissolved oxygen concentrations increased. Based on the low values of the L_N and W and

the intensity of the response, large scale upwelling and mixing by nonlinear internal waves would have led to the changes.

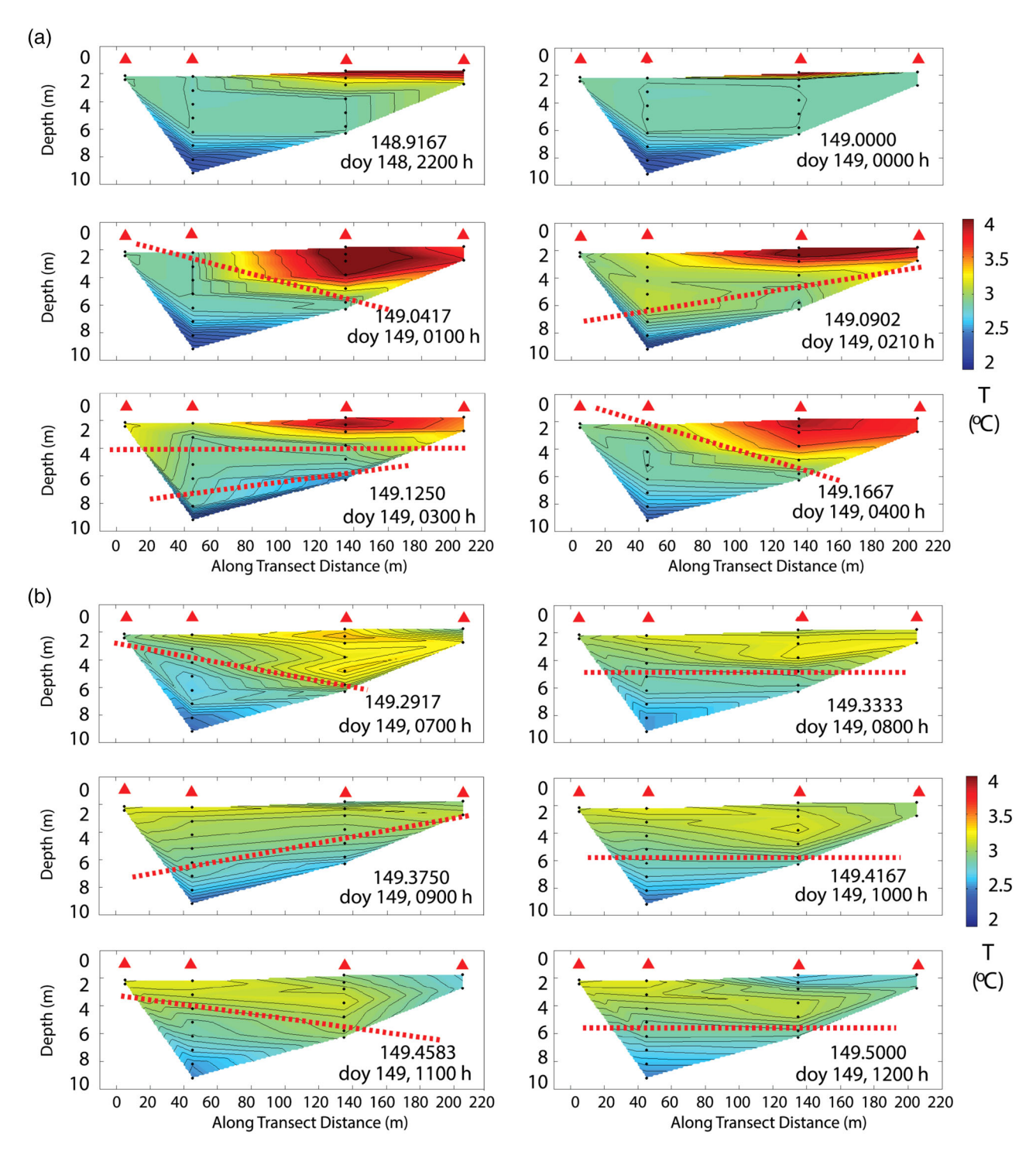


Fig. 14. Cross sections of temperature along the main axis in Lake N2 (northwest to southeast) showing upwelling and downwelling of the thermocline (red dashed line) at ice-off in 2015. Panel (**a**) illustrates heat being mixed downward immediately following ice-off; panel (**b**) illustrates continued internal wave motions, heat flowing below the surface at temperatures below 4°C as the upper water column freshened and formation of a mid-water column maximum in temperature. Increased SC in the lower water column precludes full downward mixing. Red triangles at top of panels mark the location of the thermistor arrays (Fig. 1), and black dots the depths of the loggers. Isotherms every 0.01°C. Day of year (doy), hour and decimal doy are shown in each panel.

Nonlinear waves at ice-off

To determine the extent of upwelling and the degree of nonlinearity of the internal wave field, we describe the events at ice-off using data from arrays along the west-east axis of L. N2. Due to the fresher near-surface water, the water column was stably stratified even when warmer water overlaid cooler water when temperatures were below 4°C. In L. N2 in 2015, with northwesterly winds of 6 m s⁻¹, warmer water was at the eastern side of the basin prior to midnight on doy 149 (Figs. 13 and 14a). Consequently, thermal stratification was insignificant above 6 m at the deep station to the west, T-02, whereas a pronounced thermocline was present at T-03 to the east. Internal waves in the near-surface had the classic shape of nonlinear waves, that is, they were steep fronted, exhibited rapid upwelling and downwelling, and at times highfrequency waves occurred in the troughs. Visual inspection indicated the period of the larger waves was close to 15 min. The initial wind at ice-off, ~ 149.03, was 6 m s⁻¹ and L_N dropped below 1. Upwelling occurred to the west and downwelling at T-03 (Figs. 13 and 14a). Elevated temperatures at T-04 were also indicative of the winds advecting warmer water to the east. When the wind began to decrease, the thermocline split at T-03 and the interior core was filled with highfrequency waves (doy 149.05). On cessation of the wind, downwelling of warmer water occurred at T-02 and upwelling at T-03 (~doy 149.07). Temperatures also dropped at T-04. indicating the thermocline tilted along the full lake basin. Water with temperatures slightly above 3°C spread over the lake surface. As the wind increased at 149.1, the thermocline compressed at depth at T-02 and both the upper thermocline and the chemocline upwelled at T-03. As the wind speed dropped from 5 to 2 m s⁻¹ at 149.18, the thermocline at T-03 downwelled whereas the lower thermocline at T-02 upwelled. A pattern of upwelling at the one station with downwelling at the other persisted over the next half day (Figs. 13 and 14a). While heat was initially mixed downward (Fig. 14a), nearsurface temperatures subsequently cooled from increased precipitation and the arrival of a cold front (Figs. 3, 13, and 14b). Consequently, thermal stratification in the mid-water column was less after ice-off in 2015 than in 2014 (Figs. 4 and 5, right panels). The near-bottom mixing was sufficient to erode the chemocline although chemical stratification persisted in the lower water column and the near-bottom was hypoxic.

These data from L. N2 illustrate the basin scale upwelling and downwelling that occurs with low L_N and W following ice-off. The abrupt changes in isotherm depth are indicative of nonlinear waves with the high-frequency waves often in the troughs or when the thermocline split, as at T-03, the signature of solitons. The complexity of the internal wave field increased within a few hours. For example, beginning at doy 149.28, abrupt upwelling occurred above 6 m and abrupt downwelling to 7 m with upwelling occurring below 7 m. Within less than an hour, the upper water column downwelled, upwelling occurred from 6 to 7 m, and downwelling occurred deeper in

the water column. Such behavior is indicative of 3rd vertical mode nonlinear waves. While upwelling and downwelling occurred over the next several hours, the arrival of a cold front added an additional complexity. As temperatures in the lake were below 4° C, water that warmed more rapidly in the shallows flowed below the surface and above the deeper layer which had remained chemically stratified (Fig. 14a,b). Thus, as upwelling and downwelling continued, a layer with temperatures of $\sim 3^{\circ}$ C, warmer than the water above and below, developed mid-water column.

Second vertical mode nonlinear internal waves in L. E1

Internal wave dynamics at ice-off in L. E1 in 2015 showed the intensification of mixing once wind interacted with the water surface (Fig. 7, right panels). Higher order vertical mode waves were evident after the first wind event. Similar to L. N2, a pool of water with temperatures near 5°C was near the surface such that when it was mixed downward, thermal stratification in the upper water column was pronounced. As ice-off was occurring and wind speeds reached 5 m s⁻¹, internal waves were first vertical mode (Fig. 15). When wind speeds reached 7 m s⁻¹, W, computed using a mixed layer depth of 3 m, the length of the lake along the east-west axis of 200 m, and $\Delta \rho = 0.06 \text{ kg m}^{-3}$, was 0.6, and L_N , computed from the density profile was 0.3 using full lake bathymetry and 0.5 using bathymetry for the main basin. The initial response was upwelling. As the wind dropped, it evolved into a 2nd vertical mode wave response, with the wave's upper extent reaching 2 m and the deeper downwelling reaching 9 m depth. The thermocline subsequently compressed and expanded again. These waves were steep sided which implies they are nonlinear waves. As a result, the thermocline deepened by a meter and temperatures increased in the water above. The 2nd vertical mode internal wave train continued over the next several days with a periodicity of 1.7 h in the first 12 h. This periodicity is more rapid than the 3.5 h computed for a 2nd vertical mode response following Gill (1982) using basin length at thermocline depth of 100 m. The higher frequency further supports the waves being nonlinear, with the caveat that basin shape can modify the predicted response of seiches (Fricker and Nepf 2000). The internal wave response in the deeper pycnocline included downwelling, upwelling, and formation of a wave train such that the pycnocline broadened and SC decreased. The flows indicate how the nonlinearities induced in the upper pycnocline during events with low Wedderburn number induce nonlinear internal wave responses in a lower pycnocline.

Delayed near-bottom mixing when winds are strong just prior to ice-off

The data from L. E1 in 2014 provide an example (Fig. 6, right panels). With westerlies of magnitude 7 m s $^{-1}$ on day 163 when the lake was still ice-covered, W dropped to 0.9 assuming no ice cover and that the wind acted on the full length of the lake. Near-

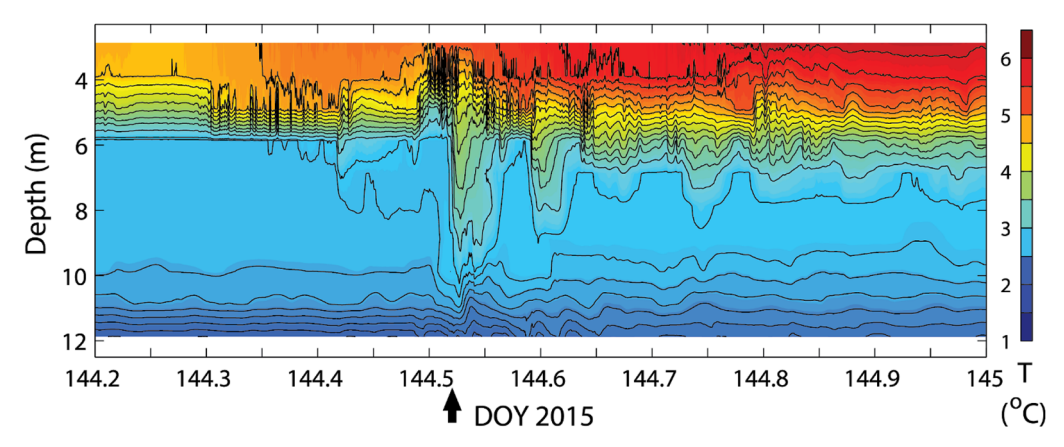


Fig. 15. Temperature time series showing the 2nd vertical mode internal waves which formed as the thermocline thickened as heat was mixed downward immediately after ice-off in Lake E1, 2015. Ice-off is indicated by an arrow.

surface temperatures decreased and those below increased indicating mixing. The thermocline descended from 2 to 6 m. Isotherms were also compressed in the lower water column implying some mixing there. At ice-off on day 165, the wind was of similar magnitude but northerly, reducing the fetch. Additionally, due to the earlier mixing event, the mixed layer was 5 m deep. Hence, rather than dropping below 1, $W \approx 3$ indicating only partial upwelling. The base of the thermocline only descended from 6 to 7.5 m. W dropped to 2 on the next windy day. 168. During this last event, the near-bottom mixing occurred that warmed the lower water column, reduced chemical stratification, and supplied oxygen. With the deepening of the thermocline under the ice, winds of a magnitude that would have caused full upwelling at ice-off for a shallower thermocline only caused partial upwelling and several events with a low value of W were required for sufficient mixing to dilute the near-bottom chemocline.

The moderate winds and weak stratification enabled upwelling and rapid downward mixing of heat in both years and in both lakes. Except in L. N2 in 2015 when ice-off was followed by a cold-front, temperatures in surface waters quickly reached 8°C after ice-off. As can be seen in Figs. 4–7 and 13–15, with the rapid heating, the window during which solutes from the lower water column could mix upward is short.

Discussion

A complex suite of interacting physical processes occurred under the ice and at ice-off in the two small arctic lakes. Most striking was the internal wave activity which was accentuated where density stratification was least. Additionally, penetrative convection, which has been critical for the downward mixing of heat in spring in most ice-covered lakes (Kirillin et al. 2012), only occurred for a brief period immediately before ice-off if at all. Several attributes of the small arctic lakes caused them to differ from many others that have been

studied (Table 1). The differences include the considerable contribution of specific conductance to density and its temporal variations, proximity of boundaries, and relatively low attenuation coefficients such that solar radiation could penetrate to the bottom or nearly to the bottom of the lakes. Between-vear differences in temperature during winter and the rapidity of snowmelt contributed to the diversity of processes. Water temperatures in the 2nd year of our study were colder and near-bottom increases in specific conductance were lower during spring in that year. Additionally, snowmelt occurred more rapidly in that year, enabling greater freshening of the upper half of the water column. These between-year differences set the stage for differences in the mode and amplitude of internal waves and the incidence of diurnal mixed layers with stable temperature stratification. Sudden warming at the base of the weakly stratified layer occurred in late spring likely due to downslope flow of water warmed in shallow regions. Near-surface pycnoclines from snowmelt and a chemocline from respiration over the winter occurred in both lakes in both years. These features restricted penetrative convection and precluded the lakes' mixing prior to ice-off. Consequently, mixing at ice-off was mediated by nonlinear internal waves.

Proximity to boundaries and depth dependent changes in specific conductance created conditions which set the two small arctic lakes apart from others which have been studied in spring. With 9 months of ice cover and cold air temperatures, the surface layer where temperatures decreased most rapidly was ~ 4 m thick and with larger temperature gradients in contrast to those in many ice-covered lakes farther south (Table 1). Specific conductance decreased below the ice providing evidence for downward mixing of solutes from cryoconcentration (Granin et al. 1999; Bluteau et al. 2017). Specific conductance then increased again by mid-water column with the largest increase near the bottom boundary. The solutes were produced by sediment respiration over the winter (Mortimer and Mackereth 1958; MacIntyre et al. 2018a). Temperatures were either weakly stratified below the

surface boundary layer or decreased below it such that a temperature maxima occurred in the mid to lower water column. When these combined conditions led to weak stratification in the mid-to lower water column, higher order vertical mode internal waves formed. The extensive mixing from penetrative convection and relatively thick ice cover has been assumed to preclude internal wave formation during Winter II except at the base of the convectively mixing layer (Kirillin et al. 2012; Bouffard et al. 2016). The prevalence of internal waves under the ice in the two small lakes was unexpected.

For the majority of ice-covered lakes in which measurements have been obtained in spring, the period Kirillin et al. (2012) call Winter II, penetrative convection has been the dominant form of RDC causing the downward movement of heat (Kirillin et al. 2012; Table 1). Interior convection was noted in one lake with a strong near-surface temperature gradient and a low attenuation coefficient (Malm et al. 1997). Our sites differed in that temperature maxima were found away from the surface that expanded in the day and contracted at night. While solar heating could cause the expansions and convection the mixing that induced nearisothermy, we argue that internal waves contributed to the pattern. In support of this mechanism, our calculations for L. N2 in 2014 indicate direct solar radiation caused the changes in temperature over diel cycles except on windy days with considerable upwelling (Fig. S2). We posit that the expansions and contractions are from 2nd vertical mode internal waves and that the apparent warming in the center of these features resulted from advection of warmer water from the nearshore. In the more highly stained lake, L. E1, 2nd vertical mode expansions were also prevalent where stratification was weak. Sloping boundaries enabled larger increases in temperature nearshore and created conditions favorable for horizontal convection and downslope flows in late spring (Stefanovic and Stefan 2002; Salonen et al. 2014). The rapid increases in temperature at the base of the weakly stratified region often occurred when winds ceased. Thus, internal wave motions may have contributed to the flows. Regardless of the mechanism, internal wave expansion and contraction would increase the rate and spatial extent of offshore flow and overall lake warming.

The extent of biological activity over the winter and during summer may determine whether penetrative convection occurs in arctic lakes. It did contribute to the downward movement of heat at arctic sites near ours (Table 1). In Lake Peters, it may have been facilitated by smaller temperature gradients in the surface layer and in L. E5 by higher attenuation coefficients and smaller gradients in solute concentration. At our sites, where density stratification persisted largely due to increases in SC from respiration, RDC was precluded. Internal waves were critical for transport of heat throughout spring and horizontal convection contributed in late spring.

In the following, we further discuss attributes of the lakes which moderated the hydrodynamics, address the unique

aspects of the internal wave field in the two small arctic lakes, and discuss strategies for future studies including adaptations to current models.

Influence of specific conductance

The differing conditions within the two years at the onset of spring warming illustrate how processes operative during winter moderate spring heating and mixing. In 2014, a minimum in specific conductance occurred mid-water column in L. N2; and SC increased below 4 m and stabilized the temperature inversion in L. E1 in both years (Fig. 2). In L. N2 in 2014, the warmest water moved progressively upward. Increases in density stratification occurred below the warm layer retarding RDC. The increase was due to increases in SC. Interestingly, a similar increase in SC occurred in Toolik Lake. With ongoing increases in CO2 under the ice in some years (MacIntyre and Cortés 2017), the increase may in part be due to continuing sediment respiration, which during winter had led to intrusions which flowed offshore at depths with similar density (MacIntyre et al. 2018a). Throughout the winter and into the spring, SC at 8.5 m slowly increased with periodic fluctuations, whereas that at 9.5 m showed a steadier increase. Downward mixing of solutes produced by cryoconcentration, as implied by the density inversion on day 133 in L. N2 in 2014 (Fig. 2) may be another source. In consequence, whether RDC can cause appreciable vertical mixing depends on the rate of increase of density in the upper water column from heating relative to the increase in density in the waters below due to increased SC derived from the sediments or elsewhere in the water column.

In all the lakes, SC contributed to density stratification, with its contribution to density less in the cold year in L. N2 such that stratification remained stronger and the internal waves that formed were first vertical mode. In L. E1 with its inverse temperature stratification below 4 m, SC enabled stable density stratification. With the weak stratification in the lower water column, internal waves were 2nd vertical mode and, with continuing chemical stratification as ice-off approached, penetrative convection was precluded. Above the 4 m pycnocline, the density stratification from SC was large enough that temperature was stably stratified. To our knowledge, layers with stable temperature stratification under the ice, such as the ones in L. E1, have not been reported previously. The appreciable influence of specific conductance on density structure under the ice, as illustrated here, may be greater in small lakes, with their greater area of sediments relative to lake volume, in lakes with considerable loading of organic matter from the landscape, in productive lakes, or in lakes with abundant macrophytes that respire or decompose over the winter.

Snowmelt and near-bottom chemoclines

The persistence of snowmelt within the lakes varied between lakes and years. In L. N2, when heating in spring occurred intermittently, much of the snowmelt exited the lake. In L. E1,

freshwater was persistently below the ice until ice-off. The increasing depth of fresher water and our heat budgets which showed smaller changes in temperature than predicted from incoming solar radiation to depths of 4 to 5 m, indicated some downward mixing of incoming snowmelt, a process abetted in L. E1 relative to L. N2 by smaller gradients in SC and presumably higher discharge given its larger watershed. When snowmelt and the thinning of the ice co-occurred, as in warm years with a rapid melt, more of the incoming meltwater would be retained to be mixed downward by wind induced mixing at ice-off. Intrusions of warmer water into the lower water column were more frequent in L. E1 than L. N2. Assuming incoming snowmelt spread horizontally over the lake as observed elsewhere (Welch and Bergmann 1985; Bengtsson 1986; Cortés et al. 2017), the greater prevalence of intrusions would be facilitated by the smaller density gradient and related ease of mixing at shallow depths in L. E1. The solutes dissolved in snowmelt vary over time, with greater concentrations, for instance of dissolved organic carbon (DOC), earlier in the melt (Cortés et al. 2017). Thus, early mixing would contribute to those solutes entering the lake. However, the moats that form around icecovered lakes consist of snowmelt from streams prior to the ice's melting sufficiently for it to flow into the lake and snowmelt coming directly from land. This water tends to be olive colored and indicative of DOC. Thus, once the ice in the moats has melted, the warmed moatwater can intrude into the lakes potentially increasing the loading of solutes.

Incoming snowmelt can induce near-bottom gravity currents. During snowmelt when a lake is ice covered, the watershed large enough relative to the lake to produce appreciable inflow, and shallow subbasins downstream, incoming snowmelt can displace the water at depth in the subbasins. Heat flux from the sediments and sediment respiration can cause warmer water with higher solute concentrations to accumulate near the bottom in shallow subbasins over the winter (Figs. 10–12). With its greater density relative to the overlying water and to incoming snowmelt, this water can be displaced rather than mix with the incoming water. Hence, as observed, gravity currents can flow into a deeper basin and intrude at depths with similar density. Shallow subbasins may also have elevated CO2 or if they are anoxic, have elevated methane. These solutes would then also flow deeper into the lake making evasion to the atmosphere more difficult. If detrital flocs have also settled, these too could flow offshore providing substrate for microbial activity or food for zooplankton in the icefree period.

The stratification within the near-bottom chemoclines determined their susceptibility to internal wave motions and mixing. Stratification, characterized as buoyancy frequency, was low relative to that found in summer although larger than that found mid-water column, ranged in both lakes from 6 to 9 cph in 2014 and 8 to 11 cph in 2015. Upwelling and downwelling with amplitudes of a meter or more were more prevalent in L. E1. These movements resulted from wind acting on

the ice and incoming snowmelt (Fig. 11). Over time, the 2nd vertical mode waves weakened the density stratification and thinned the bottom pycnocline (Fig. 10). They did not alleviate near-bottom anoxia (Figs. 4–7).

Internal waves prior to ice-off

The 1 to 1.5 m upwellings and downwellings in L. N2 and the 1 to 4 m ones in L. E1 in response to wind are appreciable in small ice covered lakes. They indicate that the pressure on the ice from wind was transmitted to the water column below. While internal waves have been noted in other ice-covered lakes, to our knowledge, L. N2 and E1 are the smallest in which they have been observed (Kirillin et al. 2012). Rotation of the internal wave field such that Kelvin waves would form is expected for all but the smallest lakes. Following Gill (1982), the phase speed of the first 3 vertical modes in L. N2 in 2014 based on profiles of N² computed using data as in Fig. 2 were 0.021, 0.012, and 0.01 m s⁻¹ giving Rossby radii of ~ 160 , 90, and 75 m. The depth of the maximum amplitude of the predicted and observed 2nd vertical mode internal waves rose as the lake warmed. The width of L. N2 at those depths is 50 m when the maximum was located at 7 m but 150 m when it was located at 4 m. These results indicate the lake was too small to support rotation of this mode at the onset of heating but that rotation may have occurred in later spring. Assuming the length of the lake is the critical dimension, the computed wave period for the 2nd vertical mode increased as the weakly stratified layer moved upward in L. N2 from ~ 7 to 14 h. However, changes in wind speed and direction tended to occur on time scales less than a day indicating the waves were wind

Reported velocities due to internal wave motions are on the scale of mm s⁻¹ (Malm et al. 1998; Rizk et al. 2014) and tracer experiments indicate they can cause dispersion in the horizontal (Bengtsson 1986). We argue that the horizontal motions due to expansions and contractions transported heat and solutes within L. N2 due to spatial differences in warming (Figs. 8 and 9; Figs. S1 and S2). The boluses of warmer water appear and disappear in the lower water column of L. E1 (Figs. 10 and 11). These changes would also result from the wave motions, and horizontal flow both from intrusions and internal wave motions contributed to the warming of the lower water column in that lake. The erosion of the bottom pycnocline in L. E1 resulted from internal wave induced mixing. Internal waves may have contributed to the offshore flow of solutes from respiration which led to increased stratification in the lower water column under the ice.

Internal waves and mixing at ice-off

Wind-induced internal waves caused mixing just prior to and immediately after ice-off. Our time series measurements along a horizontal transect in L. N2 in 2015 indicated the thermocline tilted the full length of the lake, and upwelled over at least a third of the lake. For all the lakes, the internal

waves that resulted at ice-off were initially first vertical mode and later steep-fronted 2nd vertical mode waves. Based on their shape, we infer that they are nonlinear. The computed values of the Wedderburn number indicated the waves would have been internal bores (W < 1) in which mixing would be across the thermocline lake wide or surges and solitons (1 < W < 5) such that mixing would be enhanced near the boundary (Horn et al. 2001; Boegman et al. 2005a,b). The rapid deepening of the thermocline provided further evidence for mixing from instability of nonlinear waves (Figs. 4-7, right panels). As a consequence of the intense mixing, heat was mixed deeply into the lakes. A similar shift from nonlinear first to nonlinear 2nd vertical mode waves, an abrupt descent and thickening of the thermocline, and a large introduction of heat was previously observed during strong winds during spring in a much larger lake (MacIntyre et al. 2009a). Whether this process is a general one found in all lakes in spring is unknown. Previously, for arctic lakes at least, the rapid heating at ice-off was attributed to high solar radiation, heat flux into the lakes by conduction, and low evaporation which causes heat loss (O'Brien et al. 1997; MacIntyre et al. 2009b). The pronounced upwellings and enhanced mixing expected for low values of W and L_N caused heat to be mixed deeply. Without the internal wave induced mixing, surface temperatures would be warmer and the epilimnion thinner.

Besides mixing heat downward, the mixing would also bring dissolved constituents found deeper in the water column upward. The duration of the initial period of upwelling and downwelling before heat was mixed downward is a critical time for loss of greenhouse gases produced over the winter. This period is short (Figs. 13–15), and the subsequent downward mixing of heat intensified the stratification and made mixing in the ice-free period more difficult. The internal wave induced mixing at ice-off was sufficient in most cases to weaken the near-bottom chemoclines but not to fully alleviate them. Hence, the lower water column remained hypoxic which would allow reduced compounds such as methane to persist.

Necessity for time series data and improved modeling

Predicting how thermal structure and productivity of inland waters will be moderated under climate and land use changes is a long-term goal required for developing policy that protects water quality and organisms in the lakes. The winter period is understudied, with little information on productivity and the influence of spring on the ice-free period (Hampton et al. 2016). In northern regions, a decrease in the duration of ice cover has been one of the most pronounced changes under a warming climate (Magnuson et al. 2000). With greater warming in fall in the Arctic, a similar decrease in the ice-covered period is expected. These changes will modify ice thickness, under ice temperature gradients, and the depth of the surface layer, which as shown here will influence the depth and time when convection occurs, and whether the lakes mix to the bottom before ice-off. The plasticity of the ice may vary depending on warming

and cooling cycles during winter. Under-ice temperatures at iceon and over the winter will likely vary depending on thermal stratification in summer and the duration of fall cooling (Salonen et al. 2014) as well as the duration of ice-covered period. Cooler near-bottom waters as we report here may result from heat loss to the sediments over an appreciable part of the winter or intrusions of cool more solute rich water from shallow basins. The cooling contrasts to heat gain or continued maintenance of warmer bottom temperatures as in slightly larger lakes in the Arctic (Mortimer and Mackereth 1958; Cortés et al. 2017). This difference may result from minimal heating of the sediments due to cool temperatures in the lower water column in summer in small lakes. It may also depend on the depth of the thaw bulb and the resultant temperature gradients below the lake (Tan and Zhuang 2015). As we have shown, density stratification also depends on respiration rates as they modify production of solutes under the ice (Malm et al. 1997; MacIntyre et al. 2018a). Respiration rates depend on loading of organic matter from the landscape, which will change with changes in hydrology, and, in part, on respiration by benthic algae and macrophytes (Kling et al. 1991; Karlsson et al. 2008). Loading of dissolved organic matter from the terrestrial environment will also determine attenuation coefficients and hence the buoyancy flux which initiates RDC, both influencing time of onset and depth of overturning regions. Thus, we can expect that shorter and potentially warmer winters would reduce the thermal gradient under the ice and thickness of the surface layer potentially enabling penetrative convection in these lakes. However, whether an earlier onset of RDC would alleviate anoxia will depend on sediment respiration rates as they increase stratification in the lower water column in spring. Thus, accuracy in modeling future conditions requires not only understanding how the thermal regime changes but also controls on optical conditions and sediment respiration rates.

Consistent year round measurements of temperature, specific conductance, and oxygen are required to determine the controls on under ice temperatures and density stratification. Irradiance measurements are required in all seasons. Similarly, with oxygen measurements, we are poised to quantify the extent of net heterotrophy in the ice-free and ice-covered periods and the related production of greenhouse gases (MacIntyre et al. 2018a). While studies have addressed expected changes in temperature, oxygen, or greenhouse gas production over multiple years with 1D modeling and using climate change scenarios from general climate models as inputs (Tan and Zhuang 2015), further development will include incorporating new processes such as we have shown to be important in moderating mixing dynamics in spring. Notably, the effects of respiration on density structure are required. In addition, as shown here, the use of new, high-resolution sensors enabled identification of processes and structure not previously described. These include the snowmelt-induced gravity currents and resultant near-bottom entrainment, mid-water column stratification from solutes, horizontal convection, internal wave driven transports, stable diurnal thermoclines, and, at ice-off, horizontal convection when temperatures are below 4°C, and the mixing driven by nonlinear waves within small lakes.

Improvements in hydrodynamic models, including coupling with hydrological models, are essential for future predictions. By definition, 1D models cannot capture the extensive thermocline tilting and mixing due to nonlinear waves yet including the enhanced mixing is essential. Improvements in predicting future changes also depend on modeling respiration and its influence on density structure under the ice and, including snowmelt and the extent of vertical mixing as it freshens the lakes and enables penetrative convection in later spring. While the dynamics of inflows such as snowmelt are included in 3D models, they are too time intensive to run over multiple-year periods, hence the need to improve parameterizations in 1D models. In summary, time series data of temperature and biogeochemistry are required in winter. This new knowledge is important for predicting conditions conducive to growth at all trophic levels. Consideration of the 3D flows in small water bodies is essential for accurate modeling to quantify the persistence of anoxia in the lower water column, to accurately estimate fluxes of greenhouse gases at ice-off, and to determine how conditions in winter moderate temperature and thermal structure in the ice-free season which are critical for future predictions of ecosystem structure and function.

References

- Barnes, D. F., and J. E. Hobbie. 1960. Rate of melting at the bottom of floating ice. Short Pap. Geol. Sci. U.S. Geol. Surv. Prof. Pap. **400-B**: B392–B394.
- Belzile, C., W. F. Vincent, J. A. E. Gibson, and P. Van Hove. 2001. Bio-optical characteristics of the snow, ice, and water column of a perennially ice-covered lake in the High Arctic. Can. J. Fish. Aquat. Sci. **58**: 2405–2418. doi:10.1139/cifas-58-12-2405.
- Bengtsson, L. 1986. Dispersion in ice-covered lakes. Nord. Hydrol. **17**: 151–170. doi:10.2166/nh.1986.0010.
- Bengtsson, L. 1996. Mixing in ice-covered lakes. Hydrobiologia **322**: 91–97. doi:10.1007/BF00031811.
- Bengtsson, L., J. Malm, A. Terzhevik, M. Petrov, P. Boyarinov, A. Glinsky, and N. Palshin. 1996. Field investigation of winter thermo- and hydrodynamics in a small Karelian lake. Limnol. Oceanogr. 41: 1502–1513. doi:10.4319/lo. 1996.41.7.1502.
- Bengtsson, L., and T. Svensson. 1996. Thermal regime of ice covered Swedish lakes. Nord. Hydrol. **27**: 39–56. doi:10. 2166/nh.1996.0018.
- Bluteau, C. E., R. Pieters, and G. A. Lawrence. 2017. The effects of salt exclusion during ice formation on circulation in lakes. Environ. Fluid Mech. **17**: 579–590. doi:10.1007/s10652-016-9508-6.
- Boegman, L., G. N. Ivey, and J. Imberger. 2005a. The degeneration of internal waves in lakes with sloping topography.

- Limnol. Oceanogr. **50**: 1620–1637. doi:10.4319/lo.2005.50. 5.1620.
- Boegman, L., G. N. Ivey, and J. Imberger. 2005*b*. The energetics of large-scale internal wave degeneration in lakes. J. Fluid Mech. **531**: 159–180. doi:10.1017/S0022112005003915.
- Bouffard, D., R. E. Zdorovennov, G. E. Zdorovennova, N. Pasche, A. Wuest, and A. Y. Terzhevik. 2016. Ice-covered Lake Onega: Effects of radiation on convection and internal waves. Hydrobiologia 780: 21–36. doi:10.1007/s10750-016-2915-3.
- Bouffard, D., and others. 2019. Under-ice convection dynamics in a boreal lake. Inland Waters. **9**: 142–161. doi:10. 1080/20442041.2018.1533356.
- Bruesewitz, D. A., C. C. Carey, D. C. Richardson, and K. C. Weathers. 2015. Under-ice thermal stratification dynamics of a large, deep lake revealed by high-frequency data. Limnol. Oceanogr. **60**: 347–359. doi:10.1002/lno.10014.
- Chen, C. T., and F. J. Millero. 1977. The use and misuse of pure water PVT properties for lake waters. Nature **266**: 707–708. doi:10.1038/266707a0.
- Cortés, A., S. MacIntyre, and S. Sadro. 2017. Flowpath and retention of snowmelt in an ice-covered arctic lake. Limnol. Oceanogr. **62**: 2023–2044. doi:10.1002/lno.10549.
- Duguay, C. R., G. M. Flato, M. O. Jeffries, P. Ménard, K. Morris, and W. R. Rouse. 2003. Ice-cover variability on shallow lakes at high latitudes: Model simulations and observations. Hydrol. Process. 17: 3465–3483. doi:10.1002/hyp. 1394.
- Farmer, D. M. 1975. Penetrative convection in the absence of mean shear. Q. J. Roy. Meteorol. Soc. **101**: 869–891. doi:10. 1002/qj.49710143011.
- Forrest, A. L., B. E. Laval, R. Pieters, D. S. S. Lim, D. S. S. Darlene, and D. S. S. Lim. 2008. Convectively driven transport in temperate lakes. Limnol. Oceanogr. **53**: 2321–2332. doi:10.4319/lo.2008.53.5_part_2.2321.
- Fricker, P. D., and H. M. Nepf. 2000. Bathymetry, stratification, and internal seiche structure. J. Geophys. Res **105**: 14237–14251. doi:10.1029/2000JC900060.
- Gill, A. 1982. Atmosphere-ocean dynamics. Academic Press.
- Granin, N. G., and others. 1999. Turbulent mixing in the water layer just below the ice and its role in development of diatomic algae in Lake Baikal. Dokl. Akad. Nauk **366**: 835–839
- Hampton, S. E., and others. 2016. Ecology under lake ice. Ecol. Lett **20**: 98–111. doi:10.1111/ele.12699.
- Hobbie, J. E., and others. 1995. Long-term measurements at the Arctic LTER sites, p. 397–409. *In* T. M. Powell and J. H. Steele [eds.], Ecological time series. Chapman and Hall.
- Horn, D. A., J. Imberger, and G. N. N. Ivey. 2001. The degeneration of large-scale interfacial gravity waves in lakes. J. Fluid Mech. **434**: 181–207. doi:10.1017/S0022112001003536.
- Imberger, J., and J. C. Patterson. 1990. Physical limnology. Adv. Appl. Mech. **27**: 303–473. doi:10.1016/S0065-2156 (08)70199-6.

- Jakkila, J., M. Leppäranta, T. Kawamura, K. Shirasawa, and K. Salonen. 2009. Radiation transfer and heat budget during the ice season in Lake Pääjärvi, Finland. Aquat. Ecol. 43: 681–692. doi:10.1007/s10452-009-9275-2.
- Jewson, D. H., N. G. Granin, A. A. Zhdanov, and R. Y. Y. Gnatovsky. 2009. Effect of snow depth on under-ice irradiance and growth of Aulacoseira baicalensis in Lake Baikal. Aguat. Ecol. **43**: 673–679. doi:10.1007/s10452-009-9267-2.
- Jonas, T., A. Y. Terzhevik, D. V. Mironov, and A. Wüest. 2003. Radiatively driven convection in an ice-covered lake investigated by using temperature microstructure technique. J. Geophys. Res. Ocean. 108: 3183. doi:10.1029/ 2002IC001316.
- Kalff, J. 2002. Limnology: Inland water ecosystems, 2nd ed. Prentice Hall.
- Karlsson, J., J. Ask, and M. Jansson. 2008. Winter respiration of allochthonous and autochthonous organic carbon in a subarctic clear-water lake. Limnol. Oceanogr. **53**: 948–954. doi:10.4319/lo.2008.53.3.0948.
- Kelley, D. E. 1997. Convection in ice-covered lakes: Effects on algal suspension. J. Plankton Res. **19**: 1859–1880. doi:10. 1093/plankt/19.12.1859.
- Kirillin, G. B., A. Forrest, K. Graves, A. Fischer, C. Engelhardt, and B. E. Laval. 2015. Axisymmetric circulation driven by marginal heating in ice-covered lakes. Geophys. Res. Lett. **42**: 2893–2900. doi:10.1002/2014GL062180.
- Kirillin, G., C. Engelhardt, S. Golosov, and T. Hintze. 2009. Basin-scale internal waves in the bottom boundary layer of ice-covered Lake Müggelsee, Germany. Aquat. Ecol. **43**: 641–651. doi:10.1007/s10452-009-9274-3.
- Kirillin, G., and others. 2012. Physics of seasonally ice-covered lakes: A review. Aquat. Sci. **74**: 659–682. doi:10.1007/s00027-012-0279-v.
- Kirillin, G., and A. Terzhevik. 2011. Thermal instability in freshwater lakes under ice: Effect of salt gradients or solar radiation? Cold Reg. Sci. Technol. **65**: 184–190. doi:10. 1016/j.coldregions.2010.08.010.
- Kling, G. W., G. W. Kipphut, and M. C. Miller. 1991. Arctic lakes and streams as gas conduits to the atmosphere: Implications for tundra carbon budgets. Science **251**: 298–301. doi:10.1126/science.251.4991.298.
- Luecke, C., and others. 2014. The response of lakes near the Arctic LTER to environmental change, p. 238–286. *In* J. Hobbie and G. Kling [eds.], A changing arctic: Ecological consequences for tundra, streams and lakes. Oxford Univ. Press.
- MacIntyre, S., J. F. Clark, R. Jellison, and J. P. Fram. 2009*a*. Turbulent mixing induced by nonlinear internal waves in Mono Lake, California. Limnol. Oceanogr. **54**: 2255–2272. doi:10.4319/lo.2009.54.6.2255.
- MacIntyre, S., and A. Cortés. 2017. Time series of water temperature, specific conductance, and oxygen from Toolik Lake, and Lakes E1, E5, E6, and N2, North Slope, Alaska. https://doi.org/10.18739/A2X54S

- MacIntyre, S., A. Cortés, and S. Sadro. 2018a. Sediment respiration drives circulation and production of CO₂ in ice-covered Alaskan arctic lakes. Limnol. Oceanogr.: Letters **3**: 302–310. doi:10.1002/lol2.10083.
- MacIntyre, S., A. T. Crowe, A. Cortés, and L. Arneborg. 2018*b*. Turbulence in a small arctic pond. Limnol. Oceanogr. **63**: 2337–2358. doi:10.1002/lno.10941.
- MacIntyre, S., K. M. Flynn, R. Jellison, and J. Romero. 1999. Boundary mixing and nutrient fluxes in Mono Lake, California. Limnol. Oceanogr. **44**: 512–529. doi:10.4319/lo. 1999.44.3.0512.
- MacIntyre, S., J. P. Fram, P. J. Kushner, N. D. Bettez, W. J. O. Brien, J. E. Hobbie, and G. W. Kling. 2009*b*. Climate-related variations in mixing dynamics in an Alaskan arctic lake. Limnol. Oceanogr. **54**: 2401–2417. doi:10.4319/lo.2009.54. 6_part_2.2401.
- Magnuson, J. J., and others. 2000. Historical trends in lake and river ice cover in the northern hemisphere. Science **289**: 1743–1746. doi:10.1126/science.289.5485.1743.
- Malm, J. 1998. Bottom buoyancy layer in an ice-covered lake. Water Resour. Res. **34**: 2981–2993. doi:10.1029/98WR01904.
- Malm, J., L. Bengtsson, A. Terzhevik, P. Boyarinov, A. Glinsky, N. Palshin, and M. Petrov. 1998. Field study on currents in a shallow, ice-covered lake. Limnol. Oceanogr. **43**: 1669–1679. doi:10.4319/lo.1998.43.7.1669.
- Malm, J., A. Terzhevik, L. Bengtsson, P. Boyarinov, A. Glinsky, N. Palshin, and M. Petrov. 1997. Temperature and salt content regimes in three shallow ice-covered lakes: 1. Temperature, salt content, and density structure. Hydrol. Res. 28: 99–128
- Matthews, P. C., and S. I. Heaney. 1987. Solar heating and its influence on mixing in ice-covered lakes. Freshw. Biol. **18**: 135–149. doi:10.1111/j.1365-2427.1987.tb01302.x.
- Mironov, D., A. Terzhevik, G. Kirillin, T. Jonas, J. J. Malm, and D. Farmer. 2002. Radiatively driven convection in ice-covered lakes: Observations, scaling, and a mixed layer model. J. Geophys. Res. Ocean. **107**: 7–16. doi:10.1029/2001JC000892.
- Mortimer, C. H., and F. J. H. Mackereth. 1958. Convection and its consequences in ice-covered lakes. Verhandlungen des Int. Verein Limnol. **13**: 923–932.
- O'Brien, W. J., and others. 1997. The limnology of Toolik Lake, p. 61–106. *In* A. M. Milner and M. W. Oswood [eds.], Freshwaters of Alaska. Springer New York.
- Pawlowicz, R. 2008. Calculating the conductivity of natural waters. Limnol. Oceanogr.: Methods **6**: 489–501. doi:10. 4319/lom.2008.6.489.
- Pernica, P., R. L. North, and H. M. Baulch. 2017. In the cold light of day: The potential importance of under-ice convective mixed layers to primary producers. Inland Waters **7**: 138–150. doi:10.1080/20442041.2017.1296627.
- Petrov, M. P., A. Y. Terzhevik, R. E. Zdorovennov, and G. E. Zdorovennova. 2006. The thermal structure of a shallow

- lake in early winter. Water Resour. **33**: 135–143. doi:10. 1134/S0097807806020035.
- Pieters, R., and G. A. Lawrence. 2009. Effect of salt exclusion from lake ice on seasonal circulation. Limnol. Oceanogr. **54**: 401–412. doi:10.4319/lo.2009.54.2.0401.
- Rizk, W., G. Kirillin, and M. Lepparanta. 2014. Basin-scale circulation and heat fluxes in ice-covered lakes. Limnol. Oceanogr. **59**: 445–464. doi:10.4319/lo.2014.59.2.0445.
- Salonen, K., M. Pulkkanen, P. Salmi, and R. W. Griffiths. 2014. Interannual variability of circulation under spring ice in a boreal lake. Limnol. Oceanogr. **59**: 2121–2132. doi:10. 4319/lo.2014.59.6.2121.
- Stefanovic, D. L., and H. G. Stefan. 2002. Two-dimensional temperature and dissolved oxygen dynamics in the littoral region of an ice-covered lake. Cold Reg. Sci. Technol. **34**: 159–178. doi:10.1016/S0165-232X(02)00003-4.
- Stevens, C. L., and G. A. Lawrence. 1997. Estimation of wind-forced internal seiche amplitudes in lakes and reservoirs, with data from British Columbia, Canada. Aquat. Sci. **59**: 115–134. doi:10.1007/s000270050080.
- Tan, Z., and Q. Zhuang. 2015. Methane emissions from pan-Arctic lakes during the 21st century: An analysis with process-based models of lake evolution and biogeochemistry. J. Geophys. Res. Biogeo. **120**: 2641–2653. doi:10.1002/ 2015JG003184.
- Terzhevik, A., and others. 2009. Some features of the thermal and dissolved oxygen structure in boreal, shallow ice-covered Lake Vendyurskoe, Russia. Aquat. Ecol. **43**: 617–627. doi:10. 1007/s10452-009-9288-x.
- Thorpe, S. A. 2005. The turbulent ocean, 1st ed. Cambridge Univ. Press.
- Thorpe, S. A. 2007. An introduction to ocean turbulence, 1st ed. Cambridge Univ. Press.
- Vehmaa, A., and K. Salonen. 2009. Development of phytoplankton in Lake Pääjärvi (Finland) during under-ice convective mixing period. Aquat. Ecol. **43**: 693–705. doi:10. 1007/s10452-009-9273-4.
- Welch, H. E., and M. A. Bergmann. 1985. Water circulation in small Arctic lakes in winter. Can. J. Fish. Aquat. Sci. **42**: 506–520. doi:10.1139/f85-068.
- Wüest, A., T. M. Ravens, N. G. Granin, O. Kocsis, M. Schurfer, and M. Sturm. 2005. Cold intrusions in Lake Baikal: Direct

- observational evidence for deep-water renewal. Limnol. Oceanogr. **50**: 184–196. doi:10.4319/lo.2005.50.1.0184.
- Yang, B., J. Young, L. Brown, and M. Wells. 2017. High-frequency observations of temperature and dissolved oxygen reveal under-ice convection in a large lake. Geophys. Res. Lett 44: 12,218–12,226. doi:10.1002/2017GL075373.
- Zdorovennov, R., N. Palshin, G. Zdorovennova, T. Efremova, and A. Terzhevik. 2013. Interannual variability of ice and snow cover of a small shallow lake. Est. J. Earth Sci. **62**: 26–32. doi:10.3176/earth.2013.03.
- Zdorovennova, G. E. 2009. Spatial and temporal variations of the water-sediment thermal structure in shallow ice-covered lake Vendyurskoe (Northwestern Russia). Aquat. Ecol. **43**: 629–639. doi:10.1007/s10452-009-9277-0.

Acknowledgments

The authors thank Jade Lawrence, Erik Young, Katie Ringler, Jeb Timm, Joe Franich, Adam Crowe, Caitlin Rushlow, John Lenters, and John Melack for their help with field measurements and laboratory analysis, and Adam Crowe for assistance with processing and analysis of physical data for the 2014 spring season. The authors thank Fabian Wolk and Rockland Scientific for the loan of the JFE Advantech CTD plus Rinko for the 2014 spring field season. The authors thank Jason Stuckey and Randy Fulweber for the bathymetry data and elevation maps, and the Arctic LTER for logistical support and elevation maps (National Science Foundation [NSF] DEB-1026843). John Klink provided the software for computing the modes and phase speeds of internal waves following Gill (1982). Meteorological datasets provided by the Toolik Field Station Environmental Data Center are based upon work supported by the U.S. NSF under grants 455541 and 1048361. Logistic support provided by UAF IAB Toolik Field Station was funded by NSF PLR 1048361. User days at Toolik Field Station were provided by CH2M Polar Services through the NSF's Arctic Research Support and Logistics Program grants 1204267 and 0919603. This project was supported by NSF ARC grants 1204267 and 1737411 to S.M.

Conflict of Interest None declared.

Submitted 22 November 2018 Revised 29 May 2019 Accepted 11 July 2019

Associate editor: Leon Boegman